NOMA-Assisted ISAC System: Downlink and Uplink Performance in Rician Fading Channels

Ishaan Agrawal, Harsh Raj, *Student Member, IEEE*, and B. R. Manoj, *Senior Member, IEEE*

***Abstract*— This paper analyzes the performance of the non-orthogonal multiple access (NOMA)-assisted integrated sensing and communication (ISAC) system over Rician fading channels. We consider a transceiver at the base station communicating with two downlink (DL) and uplink (UL) users while simultaneously performing mono-static target sensing in the presence of co-channel interferences. We investigate the communication performance of this system by analytically deriving the closed-form expressions of outage probabilities of near and far users in the DL and UL scenarios. Moreover, we utilize Jensen's inequality and first-order Taylor series approximation to obtain the ergodic rates of the DL and UL communication users (CUs). As a special case, we also derive closed-form expressions of the ergodic rates in the presence and absence of a target for the Rayleigh fading scenario. Furthermore, we analyze the performance of target sensing by deriving the probability of detection and false alarm. To ensure uniform quality-of-service to the near and far CUs in the UL, we have designed a communication-centric max-min power allocation optimization problem under a radar service constraint. We analyze the performance of the proposed system model in terms of outage probabilities, ergodic rates, target detection probability, and receiver operating characteristics under both Rayleigh and Rician fading scenarios, considering the impact of interference between communication and sensing functionalities. Moreover, we compare the obtained results with those of the orthogonal multiple access (OMA)-based scheme. All derived results have been validated through Monte-Carlo simulations.**

***Index Terms*— Communication-centric, ergodic rate, integrated sensing and communication (ISAC), non-orthogonal multiple access (NOMA), outage probability, Rician fading, target detection.**

I. INTRODUCTION

THE growing demand for the spectral hunger applications of modern wireless communication networks has led to frequency spectrum overcrowding and congestion problems with conventional radar systems [1]. To overcome the profusion of connected devices and utilize the radio resources efficiently, network providers seek opportunities to reuse spectrum allocated for radar due to the large portion of spectrum availability at radar frequencies [2]. Next-generation wireless communication systems are expected to integrate communication and radar sensing into a unified framework, enabling mutual enhancement between the two functions [3]. However, due to the coexistence, the interference in the radar bands increases at higher frequencies. Thus, two potential research directions exist to achieve spectrum sharing, namely: i) sensing communication coexistence (SCC) and ii) integrated sensing and communication (ISAC). The communication and radar systems in SCC coexist, separated in their location with cross-interferences between them [4]. SCC aims to develop efficient interference management techniques to facilitate the operation of the two systems and share the same spectrum. On the other hand, in ISAC, the sensing and communication functionalities are combined within a unified framework. The main objective of ISAC is to achieve smart connectivity of everything, where wireless devices are integrated with the ability to sense the environment, communicate with other user devices, and satisfy the increasing demands for ubiquitous sensing and communication (S&C) [5]. S&C share many similarities in terms of hardware, system architecture to some extent, and signal processing algorithms [6]. Therefore, without significant modifications to the existing wireless infrastructures, ISAC can help equip communication networks with sensing functionality, effectively reducing the size and cost of transceivers.

The S&C waveform design and performance analysis of ISAC employing orthogonal multiple access (OMA) techniques have been extensively studied in [7], [8], [9] and the references therein. However, the unified hardware design and resource sharing in ISAC suffer from severe inter-functionality interference, and thus achieving an effective performance trade-off between S&C is challenging [10]. In contrast, the non-orthogonal multiple access (NOMA) technique is a potential candidate for efficiently alleviating this while achieving integrated gain in terms of spectral efficiency without compromising the sensing performance. NOMA employs superposition coding at the transmitter while successive interference cancellation (SIC) is utilized at the receiver [11] and provides extra spatial degrees of freedom (DoF), distinguishing multiple users in the power domain. One of the prominent features of NOMA is its efficient interference management, which enables more effective spectrum utilization. In addition, NOMA also reduces the transmission duration compared to the time-division multiple access scheme, which is beneficial for maintaining the freshness of information,

Received 9 June 2025; revised 11 September 2025; accepted 15 October 2025. Date of publication 28 October 2025; date of current version 31 December 2025. This work was partly supported by Nokia University Donation and partly by the Start-Up Grant of the Indian Institute of Technology Guwahati. The associate editor coordinating the review of this article and approving it for publication was R. Long. *(Ishaan Agrawal and Harsh Raj contributed equally to this work.) (Corresponding author: B. R. Manoj.)*

The authors are with the Department of Electronics and Electrical Engineering, Indian Institute of Technology Guwahati, Guwahati, Assam 781039, India (e-mail: 1108.ishaan@gmail.com; h.raj@iitg.ac.in; manojbr@iitg.ac.in).

Digital Object Identifier 10.1109/TCCN.2025.3626335

especially in time-sensitive applications that are also crucial for sensing functionality [12]. These advantages of NOMA, including user fairness and flexible resource allocation, make it well-suited for ISAC, enabling shared signal usage for both communication and sensing applications such as internet-of-things (IoT) devices, vehicle-to-everything, and environment monitoring [13].

A. Related Works

A NOMA-assisted ISAC framework in the downlink (DL) scenario was proposed in [14], which showed its superiority over the conventional OMA scheme in achieving a better communication-sensing performance trade-off. The performance of the NOMA-aided ISAC system for the individual uplink (UL) and DL scenario received much attention [15], [16], [17], [18] by assuming a common waveform for both sensing and communication functionalities. In contrast, the work in [19] and the references therein utilized dedicated sensing and communication signals to avoid sensing beampattern distortion.

The works in [14], [17], [18], [19] have established a solid foundation for analyzing the performance of NOMA-assisted ISAC systems in DL scenarios, particularly in terms of the outage and ergodic rate metrics. In [15], considering communication users (CUs) and the target in a UL scenario, the authors investigated the outage probability, ergodic capacity, and sensing rate. The authors in [16] investigated the CUs' performance in the UL scenario by considering semi-ISAC networks, where a portion of the bandwidth is allocated for sensing functionality while the remaining is dedicated for communication. The works in [14], [15], [16], [17], [18], [19] provided a comprehensive overview of NOMA-assisted ISAC systems, focusing either on the DL or UL scenarios. However, in practical applications, interference from UL devices to DL devices is inevitable and causes co-channel interference. To address this issue, [20], [21] investigated the outage probabilities for CUs and examined the impact on target sensing performance, considering the interference between UL and DL transmissions in a Rayleigh fading environment. Further, in [22], the authors investigated the ergodic rate analysis for both UL and DL scenarios under a similar system and fading environment. However, such a fading scenario is impractical for sensing applications as it cannot capture the line-of-sight (LoS) paths. Assuming a non-line-of-sight (NLoS) scenario for sensing applications is a limiting factor, as it is impractical and generally, echoes from NLoS are considered as the reflections from clutter. In some typical application scenarios, such as massive machine-type communications or IoT, users are low-cost sensors deployed in a small area where both LoS and NLoS links exist, which can be practically modeled by the Rician fading channel [23]. This channel model comprises deterministic LoS and stochastic NLoS components describing the practical multipath environment. To the best of the authors' knowledge, the comprehensive performance analysis for both communication and sensing metrics by considering UL and DL CUs in the presence of a radar target employing the NOMA transmission technique over the Rician fading channel is yet to be studied, which is the motivation behind this work. Based on the aforementioned discussions, a comparison between the existing works and our proposed work is summarized in Table I.

The main contributions of this work are as follows:

(a) For CUs, we derive the analytical framework for the closed-form expressions of the outage probabilities in the DL and UL scenarios in the presence of target and co-channel interferences. We then derive asymptotic expressions for the outage probabilities in both DL and UL scenarios and analyze their behavior. We further deduce the expressions for a Rayleigh fading environment and obtain insights into the performance of the NOMA-assisted ISAC system. Since we consider the power domain NOMA, the effect of varying the fractional power coefficients is also inferred.

(b) We derive the cumulative distribution function (CDF) expressions of the CUs in both DL and UL scenarios and observe that obtaining closed-form expressions for their ergodic rates under Rician fading is mathematically intractable. Therefore, we utilize Jensen's inequality and a first-order Taylor series approximation to obtain upper bounds on the achievable rates of the DL and UL CUs. Furthermore, we derive analytical closed-form expressions for the ergodic rates in the DL scenario in the presence of a target and interference under a Rayleigh fading channel. For the UL case with Rayleigh faded channels, we derive the approximate expressions using the Gauss-Laguerre quadrature [24] method and numerically, we observe that the results obtained through these expressions exactly match the simulation results.

(c) We derive analytical expressions for the detection and false alarm probabilities to analyze the target sensing performance and receiver operating characteristics (ROC) in the presence of interference from UL CUs in the considered system model. The area under the ROC curve (AUC) is utilized to evaluate the detector performance, where a higher AUC signifies better detection capability.

(d) Finally, we formulate a communication-centric design framework to maximize the minimum achievable rate of the CUs in the UL scenario. To this end, we consider a max-min power allocation optimization problem that ensures fairness and uniform quality-of-service among the CUs, subject to the service constraint that the radar target's signal-to-interference-plus-noise ratio (SINR) remains above a given threshold. We utilize Jain's index to measure the tradeoff between the sum rate and the fairness among the CUs.

B. Notations

We use $\mathbb{E}[\cdot]$ and $\mathrm{Var}(\cdot)$ to denote the expectation and variance operators, respectively. The probability density function (PDF) and CDF of a random variable (RV) R are denoted by $p_R(r)$ and $F_R(r)$, respectively. The probability of an event is represented as $\Pr(\cdot)$. $Q_m(a,b) = \frac{1}{a^{m-1}}\int_b^\infty u^m e^{-\frac{u^2+a^2}{2}} I_{m-1}(au)\,\mathrm{d}u$ is the generalized Marcum Q-function of order m with non-centrality parameter a, where $I_{m-1}(\cdot)$ denotes the modified Bessel function of the first kind of order $m-1$. The Gaussian Q-function is denoted by $Q(u) = \frac{1}{\sqrt{2\pi}}\int_u^\infty e^{-\frac{t^2}{2}}\,\mathrm{d}t$. The complementary error function

TABLE I
COMPARISON OF EXISTING WORKS WITH THE PROPOSED NOMA-AIDED ISAC FRAMEWORK

Scenario	Reference	Channel	OP	Ergodic rate	Resource allocation	Sensing metric
Downlink	[14]	Rayleigh	✗	✗	✓	✗
	[17]		✓	✓	✗	✓
	[18]		✓	✓	✗	✓
	[19]		✗	✗	✓	✓
Uplink	[15]	Rayleigh	✓	✓	✗	✓
	[16]		✓	✓	✗	✗
Downlink & Uplink	[20]	Rayleigh	✓	✗	✗	✓
	[22]	Rayleigh	✗	✓	✗	✗
	Our work	**Rician**	✓	✓	✓	✓

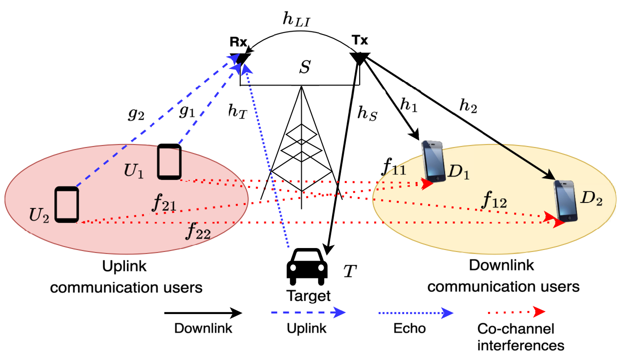

Fig. 1. NOMA-empowered ISAC system in the presence of DL and UL CUs.

is given by $\mathrm{erfc}(u) = 2Q(\sqrt{2}u)$. $L_n^{\vartheta}(\cdot)$ represents the generalized Laguerre polynomial of degree n and order ϑ. The confluent hypergeometric function of the first kind is given by ${}_1F_1(u; v; w) = \frac{\Gamma(v)}{\Gamma(v-u)\Gamma(u)} \int_0^1 e^{wt} t^{u-1}(1-t)^{v-u-1}\,\mathrm{d}t$, where $\Gamma(y) = \int_0^{\infty} t^{y-1} e^{-t}\,\mathrm{d}t$ denotes the gamma function. The natural logarithm is given by $\ln$, and the logarithmic function with base 2 is denoted as $\log(\cdot)$. The exponential integral function is given as $\mathrm{Ei}(u) = \int_{-\infty}^{u} \frac{e^{-t}}{t}\,\mathrm{d}t$.

II. SYSTEM MODEL

A. Channel Model

A NOMA-empowered ISAC system in the presence of DL and UL CUs, shown in Fig. 1, is considered, where a full-duplex (FD) base station (BS) is equipped with a single transmitting and receiving antenna. We consider two DL CUs D_1 and D_2, where the channels from the BS to these users are denoted by h_1 and h_2, respectively, with $h_i \sim \mathcal{CN}(\mu_i, \sigma^2_{D_i})$, $i \in \{1, 2\}$. Further, two UL CUs are assumed as U_1 and U_2, where the channels from these users to the BS are given by g_1 and g_2, respectively, $g_j \sim \mathcal{CN}(\mu_j, \sigma^2_{U_j})$, $j \in \{1, 2\}$. We assume that all the CUs are equipped with a single antenna. The NOMA transmission scheme is adopted for both the DL and UL scenarios. Further, we assume a target is present in the environment, the channel from BS to target and the channel of reflected echo from target to BS is denoted as $h_S \sim \mathcal{CN}(\mu_S, \sigma^2_S)$ and $h_T \sim \mathcal{CN}(\mu_T, \sigma^2_T)$, respectively. As the BS is an FD transceiver, we denote the loop self-interference channel by h_{LI}. The co-channel interferences from $U_1 \to D_1$, $U_2 \to D_1$, $U_1 \to D_2$, and $U_2 \to D_2$ are denoted by f_{11}, f_{21}, f_{12} and f_{22}, respectively, with $f_{ij} \sim \mathcal{CN}(\mu_{ij}, \sigma^2_{ij}), i, j \in \{1, 2\}$. We have considered non-zero mean for all the channels since they undergo Rician fading distribution [25]. In the DL and UL scenarios, the near CUs are denoted by D_1 and U_1, respectively, whereas the far CUs are denoted by D_2 and U_2, respectively. The channel variance is given by $\sigma^2_{\epsilon} = g(1 + d_{\epsilon}^{\nu})^{-0.5}$, where g is a complex Gaussian RV with non-zero mean and unit variance, with $g \in \{h_i, g_j, h_S, h_T, f_{ij}\}$ and $\epsilon \in \{D_1, D_2, U_1, U_2, S, T, ij\}, i, j \in \{1, 2\}$; d_{ϵ} represents distance between the nodes and ν denotes the pathloss exponent. We assume $Y \in \{h_i, g_j, h_S, h_T, f_{ij}\}, i, j \in \{1, 2\}$; the PDF of $|Y|^2$ follows non-central chi-square distribution with 2 DoF given by

$$p_{|Y|^2}(y) = \frac{1}{\mathrm{Var(Y)}} \exp\left(-\frac{s^2 + y}{\mathrm{Var(Y)}}\right) I_0\left(\frac{2s\sqrt{y}}{\mathrm{Var(Y)}}\right), \quad (1)$$

where $s^2 = m_1^2 + m_2^2$, m_1 and m_2 denote the means of two independent Gaussian distributed RVs and the variance is $\frac{\mathrm{Var}(Y)}{2}$.

B. Signal Model

We employ the NOMA technique, utilizing the superposition-coded information signal transmitted by the BS to communicate with the DL near and far CUs while simultaneously detecting the radar target, which is given by $x = \sqrt{\alpha P} x_1 + \sqrt{(1-\alpha)P} x_2$, where α and $1 - \alpha$ are the fractional power allocation coefficients of D_1 and D_2, respectively, with $\alpha \in (0, 1)$ and x_1, x_2 are the symbols transmitted with zero mean and unit variances. The total available power at the BS is given by P. The signals transmitted by the UL near and far CUs, U_1 and U_2 are $s_1 = \sqrt{P_1} y_1$ and $s_2 = \sqrt{P_2} y_2$, respectively, where P_1 and P_2 represent their transmit powers, and y_1, y_2 are the symbols transmitted with zero mean and unit variances. The DL received signal at D_i can be written as

$$r_i = (h_i + \beta_{D_i})x + f_{1i}s_1 + f_{2i}s_2 + z_i\,, \quad (2)$$

where $i \in \{1, 2\}$ and $z_i \sim \mathcal{CN}(0, \sigma^2)$ is the additive white Gaussian noise (AWGN) at the user D_i. As a result of the reflection of the transmitted signal by the BS via the target, the sensing-to-CUs interference channels are denoted by β_{D_1} and β_{D_2}, where $\beta_{D_i} \sim \mathcal{CN}(0, \zeta^2_{D_i})$, $i = 1, 2$. In the UL scenario, the BS receives information signals from U_1 and U_2, along with the sensing echo from the target. Thus, the received signal at the BS is given by

$$r_{BS} = (g_1 + \beta_{U_1})s_1 + (g_2 + \beta_{U_2})s_2 + (\eta h + h_{LI})x + z\,, \quad (3)$$

where $z \sim \mathcal{CN}(0, \sigma^2)$ is the AWGN at the BS, η denotes the scattering coefficient of the target, and $h = h_S h_T$ represents the effective channel from BS-target-BS. The reflection of the signals transmitted by the UL CUs via the target result in the interference channels, which are specified by β_{U_1} and β_{U_2}, where $\beta_{U_i} \sim \mathcal{CN}(0, \zeta_{U_i}^2)$, $i = 1, 2$.

C. Signal-to-Interference-Plus-Noise Ratio

In the DL scenario, by applying the principle of NOMA, the near-user D_1 first decodes x_2. The SINR at D_1 to decode x_2 can be written as

$$\gamma_{2,D_1} = \frac{(1-\alpha)|h_1|^2 P}{(\alpha|h_1|^2 + \zeta_{D_1}^2)P + |f_{11}|^2 P_1 + |f_{21}|^2 P_2 + \sigma^2}\,, \quad (4)$$

Further, D_1 removes the symbol x_2 by applying SIC and then decodes its own symbol x_1. Thus, the SINR at D_1 to decode x_1 is given by

$$\gamma_{1,D_1} = \frac{\alpha|h_1|^2 P}{\zeta_{D_1}^2 P + |f_{11}|^2 P_1 + |f_{21}|^2 P_2 + \sigma^2}\,. \quad (5)$$

The far user D_2 only decodes x_2, treating x_1 as interference. Therefore, the SINR at D_2 to decode x_2 can be expressed as

$$\gamma_{2,D_2} = \frac{(1-\alpha)|h_2|^2 P}{(\alpha|h_2|^2 + \zeta_{D_2}^2)P + |f_{12}|^2 P_1 + |f_{22}|^2 P_2 + \sigma^2}\,. \quad (6)$$

In the UL scenario, the BS first decodes the symbol y_1 of near user U_1. The SINR at the BS due to U_1 can be written as

$$\gamma_{1,U_1} = \frac{|g_1|^2 P_1}{(|g_2|^2 + \zeta_{U_2}^2)P_2 + \zeta_{U_1}^2 P_1 + (\eta^2|h|^2 + |h_{LI}|^2)P + \sigma^2}\,. \quad (7)$$

After successfully decoding y_1 (strong user symbol), the BS subtracts it before decoding the far user's signal y_2. The SINR at the BS due to U_2 can be obtained as

$$\gamma_{2,U_2} = \frac{|g_2|^2 P_2}{\zeta_{U_1}^2 P_1 + \zeta_{U_2}^2 P_2 + (\eta^2|h|^2 + |h_{LI}|^2)P + \sigma^2}\,. \quad (8)$$

III. Communication Performance Analysis

In this section, we derive the analytical framework for the outage probability (OP) and the ergodic rate to evaluate the communication performance of the considered NOMA-assisted ISAC system. The OP effectively captures the impact of small-scale fading, receiver noise, and interference on the received SINR in the given environment; hence, this metric is used for determining link reliability. In contrast, the ergodic rate quantifies the average achievable rate by considering all possible fading conditions of a wireless system [26]. This metric reflects the average data transmission rate over a communication channel, which varies with received SINR and is affected by interference and fading. Specifically, we obtain the analytical expressions for these performance metrics for the near and far CUs in the DL and UL scenarios.

A. Outage Probability

1) Downlink Transmission: An outage event occurs at the far user D_2 if its symbol x_2 cannot be successfully decoded. Thus, the outage probability at D_2 can be given as

$$\overline{\mathrm{P}}_{D_2} = \Pr(\gamma_{2,D_2} \le \gamma_{22})\,, \quad (9)$$

where γ_{22} is the threshold SINR.

Theorem 1: The closed-form expression of the OP at the far user D_2 in a Rician fading channel is expressed as:

$$\overline{\mathrm{P}}_{D_2} = \sum_{k=0}^{\infty} e^{-\frac{s^2}{\sigma_{D_2}^2}} \frac{(-1)^k}{\Gamma(k+2)} L_k^0\left(\frac{s^2}{\sigma_{D_2}^2}\right)\left(\frac{\theta}{\sigma_{D_2}^2}\right)^{k+1} \mathcal{C}\,, \quad (10)$$

where $\theta = \gamma_{22}[(1-\alpha-\alpha\gamma_{22})\rho]^{-1}$ and $\mathcal{C} = c_1 + c_2 + c_3$ with $c_1 = (\rho\zeta_{D_2}^2 + 1)^{k+1}$,
$c_2 = (k+1)(\rho\zeta_{D_2}^2 + 1)^k \left[\rho_1(s^2 + \sigma_{12}^2) + \rho_2(s^2 + \sigma_{22}^2)\right]$,
$c_3 = \rho_1\rho_2 k(k+1)(\rho\zeta_{D_2}^2 + 1)^{k-1}(s^2 + \sigma_{12}^2)(s^2 + \sigma_{22}^2)$. The transmit signal-to-noise rate (SNR) of BS, U_1, and U_2 are denoted by $\rho = \frac{P}{\sigma^2}$, $\rho_1 = \frac{P_1}{\sigma^2}$, and $\rho_2 = \frac{P_2}{\sigma^2}$, respectively.

Proof: To prove Theorem 1, we solve $\Pr(\gamma_{2,D_2} \le \gamma_{22}) =$

$$= \Pr\left(\frac{(1-\alpha)|h_2|^2\rho}{(\alpha|h_2|^2 + \zeta_{D_2}^2)\rho + |f_{12}|^2\rho_1 + |f_{22}|^2\rho_2 + 1} \le \gamma_{22}\right)$$
$$= \Pr\left(|h_2|^2 \le \frac{\gamma_{22}(\rho\zeta_{D_2}^2 + |f_{12}|^2\rho_1 + |f_{22}|^2\rho_2 + 1)}{(1-\alpha(1+\gamma_{22}))\rho}\right)\,. \quad (11)$$

We know that $|h_2|^2$, $|f_{12}|^2$, and $|f_{22}|^2$ follow non-central chi-square distribution with 2 DoF. Thus, (11) can be written as

$$= \int_0^{\infty} p_{|f_{22}|^2}(w) \int_0^{\infty} p_{|f_{12}|^2}(v) \int_0^{\mathcal{A}} p_{|h_2|^2}(u)\,\mathrm{d}u\,\mathrm{d}v\,\mathrm{d}w\,, \quad (12)$$

where $\mathcal{A} = \frac{\gamma_{22}(\rho\zeta_{D_2}^2 + v\rho_1 + w\rho_2 + 1)}{(1-\alpha(1+\gamma_{22}))\rho}$. By utilizing the CDF of non-central chi-square distributed RV, we obtain

$$= \int_0^{\infty} p_{|f_{22}|^2}(w) \int_0^{\infty} p_{|f_{12}|^2}(v)\left(1 - Q_1(a,b)\right)\,, \quad (13)$$

where $a = \sqrt{\frac{2s^2}{\sigma_{D_2}^2}}$ and $b = \sqrt{\frac{2\mathcal{A}}{\sigma_{D_2}^2}}$. To solve the integrals in (13), we use infinite series expansion to make the integration mathematically tractable. Specifically, we express $Q_1(a,b)$ as an infinite series of Laguerre polynomial [27, (2.6)] as

$$\overline{\mathrm{P}}_{D_2} = \int_0^{\infty} p_{|f_{22}|^2}(w) \int_0^{\infty} p_{|f_{12}|^2}(v) \sum_{k=0}^{\infty} e^{-\frac{a^2}{2}} \frac{(-1)^k}{\Gamma(k+2)} \times L_k^0\left(\frac{a^2}{2}\right)\left(\frac{b^2}{2}\right)^{k+1}\,. \quad (14)$$

By utilizing the binomial approximation in (15), as shown at the bottom of the next page, and further solving the integrals by applying [28, (2) and (7)], we obtain the final expression as given in (10). Hence proved.

We employed an infinite series expansion to derive (10) and verified its convergence. The convergence of (10) with the numerical integration in (12) is observed for $k \ge 30$, thereby confirming the accuracy of the derived expression. The chosen infinite series expression is effective because it simplifies complex integrals into an analytically tractable representation. As observed from (10), the OP of D_2 is a function of the interference caused by the radar echo and co-channel UL CUs, where the OP saturates with the increase in k and the transmit power P. Further, we obtain the asymptotic OP expression for the D_2, as given by

$$\overline{\mathrm{P}}_{D_2}^{\infty} = 1 - Q_1\left(\frac{\sqrt{2}s}{\sigma_{D_2}}, \frac{\sqrt{2\gamma_{22}\zeta_{D_2}^2}}{\sqrt{(1-\alpha(1+\gamma_{22}))}\sigma_{D_2}}\right). \quad (16)$$

Special Case: On substituting $s = 0$ in (1), the PDFs of $|h_2|^2$, $|f_{12}|^2$, and $|f_{22}|^2$ follow central chi-square distribution with 2 DoF. Further, after solving the integrals in (12), the closed-form expression of the OP at D_2 for a Rayleigh fading channel can be obtained as

$$\overline{\mathrm{P}}_{D_2} = 1 - \frac{\sigma_{D_2}^4}{(\sigma_{D_2}^2 + \rho_2\theta\sigma_{22}^2)(\sigma_{D_2}^2 + \rho_1\theta\sigma_{12}^2)} e^{\frac{-\theta(\rho\zeta_{D_2}^2+1)}{\sigma_{D_2}^2}}. \quad (17)$$

The outage occurs at the near user if either of the symbols x_1 or x_2 is not successfully decoded at D_1,

$$\overline{\mathrm{P}}_{D_1} = 1 - \Pr(\gamma_{2,D_1} > \gamma_{22}, \gamma_{1,D_1} > \gamma_{11}), \quad (18)$$

where γ_{11} represents the threshold SINR.

Theorem 2: The closed-form expression of OP at the near user D_1 for a Rician fading channel is expressed as

$$\overline{\mathrm{P}}_{D_1} = \sum_{k=0}^{\infty} e^{-\frac{s^2}{\sigma_{D_1}^2}} \frac{(-1)^k}{\Gamma(k+2)} L_k^0\left(\frac{s^2}{\sigma_{D_1}^2}\right)\left(\frac{X}{\sigma_{D_1}^2}\right)^{k+1} \widetilde{\mathcal{C}}, \quad (19)$$

where $X = \max(\theta, \gamma_{22}(\alpha\rho)^{-1})$ and $\widetilde{\mathcal{C}} = c_4 + c_5 + c_6$, with $c_4 = (\rho\zeta_{D_1}^2 + 1)^{k+1}$, $c_5 = (k+1)(\rho\zeta_{D_1}^2 + 1)^k\left[\rho_1(s^2+\sigma_{11}^2) + \rho_2(s^2+\sigma_{21}^2)\right]$, and $c_6 = \rho_1\rho_2 k(k+1)(\rho\zeta_{D_1}^2+1)^{k-1}(s^2+\sigma_{11}^2)(s^2+\sigma_{21}^2)$.

Remark 1: An increase in the variance of sensing-to-DL CU interference channel, $\zeta_{D_i}^2$, where $i \in \{1, 2\}$, along with higher UL transmit SNRs ρ_1 and ρ_2, results in stronger interference at both the NU and FU, which, in turn, leads to degradation in their outage performance.

Proof: To prove Theorem 2, we solve (18) by simplifying the two linear inequalities as (i) $\gamma_{2,D_1} > \gamma_{22} =$

$$= \frac{(1-\alpha)|h_1|^2\rho}{(\alpha|h_1|^2 + \zeta_{D_1}^2)\rho + |f_{11}|^2\rho_1 + |f_{21}|^2\rho_2 + 1} > \gamma_{22}$$
$$= |h_1|^2 > \frac{\gamma_{22}(\rho\zeta_{D_1}^2 + |f_{11}|^2\rho_1 + |f_{21}|^2\rho_2 + 1)}{(1-\alpha(1+\gamma_{22}))\rho}. \quad (20)$$

and (ii) $\gamma_{1,D_1} > \gamma_{11} =$

$$= \frac{\alpha|h_1|^2\rho}{\rho\zeta_{D_1}^2 + |f_{11}|^2\rho_1 + |f_{21}|^2\rho_2 + 1} > \gamma_{11}$$
$$= |h_1|^2 > \frac{\gamma_{11}(\rho\zeta_{D_1}^2 + |f_{11}|^2\rho_1 + |f_{21}|^2\rho_2 + 1)}{\alpha\rho}. \quad (21)$$

Since γ_{2,D_1} and γ_{1,D_1} are dependent as evident from (18), we reformulate the inequality in terms of the RV $|h_1|^2$, as shown in (20) and (21), where $|h_1|^2$, $|f_{11}|^2$, and $|f_{21}|^2$ follow non-central chi-square distribution. Following a similar approach to solve (12) as in the proof of Theorem 1, we get (19). ■

The asymptotic OP for the user D_1 can be obtained as

$$\overline{\mathrm{P}}_{D_1}^{\infty} = 1 - Q_1\left(\frac{\sqrt{2}s}{\sigma_{D_1}}, \frac{\sqrt{2\mathcal{G}}}{\sigma_{D_1}}\right), \quad (22)$$

where $\mathcal{G} = \max\left\{\frac{\gamma_{22}\zeta_{D_1}^2}{(1-\alpha(1+\gamma_{22}))}, \frac{\gamma_{11}\zeta_{D_1}^2}{\alpha}\right\}$.

Special Case: By substituting $s = 0$ in (1) and following the similar approach as in (17), the exact OP at D_1 for a Rayleigh fading channel can be obtained as

$$\overline{\mathrm{P}}_{D_1} = 1 - \frac{\sigma_{D_1}^4 e^{-\frac{X(\rho\zeta_{D_1}^2+1)}{\sigma_{D_1}^2}}}{(\sigma_{D_1}^2 + \rho_2 X\sigma_{21}^2)(\sigma_{D_1}^2 + \rho_1 X\sigma_{11}^2)}. \quad (23)$$

2) Uplink Transmission: The near user U_1 is said to be in an outage if y_1 is not successfully decoded at the BS. Therefore, the outage probability of U_1 at the BS is given by

$$\overline{\mathrm{P}}_{U_1} = \Pr(\gamma_{1,U_1} \leq \lambda_{11}), \quad (24)$$

where λ_{11} represents the SINR threshold. Without loss of generality, it is assumed that the transmitting and receiving antennas of the BS are spatially separated; thus, the loop self-interference (LSI) can be ignored.

Theorem 3: The OP of U_1 for a Rician channel is expressed as shown in (25), as shown at the bottom of the next page, where $\widetilde{\theta} = \frac{\lambda_{11}}{\rho_1}$ and $\xi = \rho_1\zeta_{U_1}^2 + \rho_2\zeta_{U_2}^2 + 1$. The jth and lth moment of the non-central chi-square distributed RV $|g_2|^2$ and $|h|^2$, respectively, with 2 DoF, denoted by V^j and W^l, are given by

$$\mathbb{E}[V^j] = j!\,(\sigma_{U_2}^2)^j\, e^{-\frac{s^2}{\sigma_{U_2}^2}}\, {}_1F_1\left(1+j; 1; \frac{s^2}{\sigma_{U_2}^2}\right), \quad (26)$$

$$\mathbb{E}[W^l] = l!\,(\sigma_S^2)^l\, e^{-\frac{s^2}{\sigma_S^2}}\, {}_1F_1\left(1+l; 1; \frac{s^2}{\sigma_S^2}\right). \quad (27)$$

Proof: To prove Theorem 3, we solve $\Pr(\gamma_{1,U_1} \leq \lambda_{11}) =$

$$= \Pr\left(\frac{|g_1|^2\rho_1}{(|g_2|^2 + \zeta_{U_2}^2)\rho_2 + \zeta_{U_1}^2\rho_1 + \eta^2|h|^2\rho + 1} \leq \lambda_{11}\right)$$
$$= \Pr\left(|g_1|^2 \leq \frac{\lambda_{11}((|g_2|^2+\zeta_{U_2}^2)\rho_2 + \rho_1\zeta_{U_1}^2 + \rho\eta^2|h|^2+1)}{\rho_1}\right). \quad (28)$$

In the UL case, the received signal at the BS also includes the echo from the target. Thus, we need to determine the PDF of the cascaded channel BS-target-BS h such that $|h|^2 = |h_S|^2|h_T|^2$, where $|h_S|^2$ (and $|h_T|^2$) follows a non-central chi-square distribution. Assuming channel reciprocity $|h_S|^2 = |h_T|^2$ and $\sigma_S^2 = \sigma_T^2$, the CDF of $|h|^2$ is defined as

$$\overline{\mathrm{P}}_{D_2} = \sum_{k=0}^{\infty} e^{-\frac{s^2}{\sigma_{D_2}^2}} \frac{(-1)^k}{\Gamma(k+2)} L_k^0\left(\frac{s^2}{\sigma_{D_2}^2}\right) \frac{\gamma_{22}(\rho\zeta_{D_2}^2+1)}{(1-\alpha(1+\gamma_{22}))\rho\sigma_{D_2}^2} \int_0^{\infty} p_{|f_{22}|^2}(w) \int_0^{\infty} p_{|f_{12}|^2}(v) \left(\frac{\gamma_{22}(w\rho_1 + v\rho_2)}{(1-\alpha(1+\gamma_{22}))\rho\sigma_{D_2}^2}\right)^{k+1}. \quad (15)$$

$F_{|h|^2}(t) = \Pr(|h|^2 \leq t)$. Further, $F_{|h|^2}(t) = F_{|h_S|^2}(\sqrt{t})$, and the PDF of $|h|^2$ can be obtained as

$$p_{|h|^2}(t) = \frac{1}{2\sqrt{t}} p_{|h_S|^2}(\sqrt{t}) = \frac{1}{2\sqrt{t}\sigma_S^2} e^{-\frac{(s^2+\sqrt{t})}{\sigma_S^2}} I_0\left(\frac{2st^{\frac{1}{4}}}{\sigma_S^2}\right). \tag{29}$$

Therefore, (28) can be expressed as

$$= \int_0^\infty p_{|h|^2}(w) \int_0^\infty p_{|g_2|^2}(v) \int_0^{\mathcal{B}} p_{|g_1|^2}(u)\, \mathrm{d}u\, \mathrm{d}v\, \mathrm{d}w, \tag{30}$$

where $\mathcal{B} = \frac{\lambda_{11}((v+\zeta_{U_2}^2)\rho_2+\rho_1\zeta_{U_1}^2+\rho\eta^2 w+1)}{\rho_1}$. By expressing the CDF of a non-central chi-square distributed RV in terms of a Laguerre polynomial similar to (14) and applying binomial theorem [29], the integrals in (30) can be solved using [30, (2.47)] to obtain the final expression as given in (25). ■

Further, we derive the asymptotic expression for the OP of user U_1, given as

$$\overline{\mathrm{P}}_{U_1}^{\infty} = 1 - 2\exp\left(-\frac{s^2}{\sigma_{U_2}^2}\right)\left[\exp\left(\frac{s^2}{\sigma_{U_1}^2}\right) \times Q_1\left(\frac{\sqrt{2}s}{\sqrt{\sigma_{U_1}^2+\sigma_{U_2}^2}}, \mathcal{Z}_1\right) - \mathcal{Z}_2\mathcal{Z}_3 I_0(\mathcal{Z}_4)\right], \tag{31}$$

where $\mathcal{Z}_1 = \frac{\sqrt{2}s+\sigma_{U_1}\sqrt{\lambda_{11}(\zeta_{U_2}^2+\zeta_{U_1}^2)}}{\sqrt{\sigma_{U_2}^2+\sigma_{U_1}^2}}$, $\mathcal{Z}_2 = \frac{\sigma_{U_2}^2}{(\sigma_{U_2}^2+\sigma_{U_1}^2)}$, $\mathcal{Z}_3 = \exp\left(\frac{s^2(\sigma_{U_1}^2-\sigma_{U_2}^2)}{\sigma_{U_2}^2(\sigma_{U_2}^2+\sigma_{U_1}^2)}\right)$, and $\mathcal{Z}_4 = \frac{2s^2+\sigma_{U_2}^2\sqrt{8}s\sqrt{\lambda_{11}(\zeta_{U_2}^2+\zeta_{U_1}^2)}}{(\sigma_{U_2}^2+\sigma_{U_1}^2)}$.

Special Case: By substituting $s = 0$ (Rayleigh fading) in (29), $|h_S|^2$ follows central chi-square distribution, thus, the PDF becomes

$$p_{|h|^2}(t) = \frac{1}{2\sqrt{t}\sigma_S^2} e^{-\frac{\sqrt{t}}{\sigma_S^2}}. \tag{32}$$

Substituting the PDFs of $|g_1|^2$ and $|g_2|^2$ which follow central-chi square distribution, and the PDF of $|h|^2$, in (32) into (30), and then solving the integrals by utilizing [29, (3.322.2)], the closed-form expression for the OP of U_1 in a Rayleigh fading channel can be obtained as

$$\overline{\mathrm{P}}_{U_1} = 1 - \frac{\sigma_{U_1}^2\sqrt{\frac{\pi\sigma_{U_1}^2}{\eta^2\rho\tilde{\theta}}}\, e^{\frac{\sigma_{U_1}^2}{4\eta^2\rho\tilde{\theta}\sigma_S^4}}}{\sigma_S^2(\sigma_{U_1}^2+\rho_2\tilde{\theta}\sigma_{U_2}^2)} Q\left(\frac{1}{\sigma_S^2}\sqrt{\frac{2\sigma_{U_1}^2}{\eta^2\rho\tilde{\theta}}}\right). \tag{33}$$

An outage event for the far user U_2 occurs if the symbols y_1 or y_2 cannot be decoded successfully at the BS. The OP of U_2 can be formulated as

$$\overline{\mathrm{P}}_{U_2} = 1 - \Pr(\gamma_{1,U_1} > \lambda_{11}, \gamma_{2,U_2} > \lambda_{22}), \tag{34}$$

where λ_{22} is the threshold SINR.

Theorem 4: The closed-form expression for the OP of U_2 for a Rician fading channel is obtained as

$$\overline{\mathrm{P}}_{U_2} = 1 - (\mathcal{F}_1 - (\mathcal{F}_2 + \mathcal{F}_3 + \mathcal{F}_4 + \mathcal{F}_5)), \tag{35}$$

where $\mathcal{F}_i, i \in \{1,2,3,4,5\}$ in (36)-(40), as shown at the bottom of the next page. In these equations, $\mathbb{E}[W^l]$ denotes the lth moment of non-central chi-square distributed RV $|h|^2$ with 2 DoF.

Remark 2: The OP of the UL NU and FU depends on the UL transmit SNRs, DL transmit power, target scattering coefficient, and the variance of the interference channel corresponding to the signal reflected by the UL CUs via the target, where higher values of these parameters lead to a degradation in outage performance.

Proof: To prove Theorem 4, we first substitute (7) and (8) in (34), where (34) can now be re-written as

$$\overline{\mathrm{P}}_{U_2} = 1 - \int_0^\infty p_{|h|^2}(w) \int_{\mathcal{J}}^\infty p_{|g_2|^2}(v) \int_{\mathcal{B}}^\infty p_{|g_1|^2}(u)\, \mathrm{d}u\, \mathrm{d}v\, \mathrm{d}w, \tag{41}$$

where $\mathcal{B} = \frac{\lambda_{11}((v+\zeta_{U_2}^2)\rho_2+\rho_1\zeta_{U_1}^2+\rho\eta^2 w+1)}{\rho_1}$ and $\mathcal{J} = \frac{\lambda_{22}(\xi+\eta^2\rho w)}{\rho_2}$. We can simplify (41) as

$$\overline{\mathrm{P}}_{U_2} = 1 - \int_0^\infty p_{|h|^2}(w) \underbrace{\int_{\mathcal{J}}^\infty p_{|g_2|^2}(v)\, Q_1(a,b)\, \mathrm{d}v}_{\mathcal{I}_1} \mathrm{d}w, \tag{42}$$

where $a = \sqrt{\frac{2}{\sigma_{U_1}^2}}s$ and $b = \sqrt{\frac{2\mathcal{B}}{\sigma_{U_1}^2}}$. By expressing Marcum Q-function in terms of the Laguerre polynomial as similarly applied in (14), $\mathcal{I}_1$ becomes

$$\mathcal{I}_1 = \frac{e^{-\frac{s^2}{\sigma_{U_2}^2}}}{\sigma_{U_2}^2}\Bigg\{\int_{\mathcal{J}}^\infty e^{-\frac{v}{\sigma_{U_2}^2}} I_0\left(\frac{2s\sqrt{v}}{\sigma_{U_2}^2}\right)\mathrm{d}v - \sum_{n_1=0}^\infty \frac{(-1)^{n_1}}{\Gamma(n_1+2)} \times \frac{e^{-\frac{s^2}{\sigma_{U_1}^2}} L_{n_1}^0\left(\frac{s^2}{\sigma_{U_1}^2}\right)}{\sigma_{U_1}^{2(n_1+1)}} \int_{\mathcal{J}}^\infty \mathcal{B}^{n_1+1} e^{-\frac{v}{\sigma_{U_2}^2}} I_0\left(\frac{2s\sqrt{v}}{\sigma_{U_2}^2}\right)\mathrm{d}v\Bigg\}. \tag{43}$$

On solving $\mathcal{I}_1$ with the help of [28, (2) and (7)], we obtain (44), as shown at the bottom of the next page, where $\omega_1 = \sqrt{\frac{2}{\sigma_{U_2}^2}}s$, $\omega_2 = \sqrt{\frac{2\mathcal{B}}{\sigma_{U_2}^2}}$, and $\omega_3 = \frac{2s\sqrt{\mathcal{B}}}{\sigma_{U_2}^2}$. From (44), $\mathcal{I}_1$ can then be expressed as

$$\mathcal{I}_1 = \mathcal{M}_1 - \mathcal{M}_2[\mathcal{M}_3 + \mathcal{M}_4\{\mathcal{M}_5 + \mathcal{M}_6\}]. \tag{45}$$

Upon substituting (45) into (42) and solving the integral with the help of [25, (2.3.31)], [28, (2) and (7)], and [30, (2.47)], we obtain (36)-(40), which are further substituted in (35) to obtain the final expression of the OP of U_2. ■

$$\overline{\mathrm{P}}_{U_1} = \sum_{k=0}^\infty \sum_{j=0}^{k+1} \sum_{l=0}^{k+1-j} e^{-\frac{s^2}{\sigma_{U_1}^2}} \frac{(-1)^k}{\Gamma(k+2)} L_k^0\left(\frac{s^2}{\sigma_{U_1}^2}\right)\left(\frac{\tilde{\theta}}{\sigma_{U_1}^2}\right)^{k+1}\binom{k+1}{j}\binom{k+1-j}{l}\rho_2^j \xi^{k+1-j-l}(\rho\eta^2)^l \mathbb{E}[V^j]\mathbb{E}[W^l]. \tag{25}$$

Similar to U_1, we derive the asymptotic expression for the OP of far user U_2, expressed as

$$\overline{\mathrm{P}}_{U_2}^{\infty} = Q_1\left(\frac{\sqrt{2}s}{\sigma_{U_2}}, \frac{\sqrt{2(\lambda_{22}(\zeta_{U_2}^2+\zeta_{U_1}^2))}}{\sigma_{U_2}}\right) - 2\exp\left(-\frac{s^2}{\sigma_{U_2}^2}\right) \times\left[\exp\left(\frac{s^2}{\sigma_{U_1}^2}\right)Q_1\left(\frac{\sqrt{2}s}{\sqrt{\sigma_{U_1}^2+\sigma_{U_2}^2}}, \mathcal{Z}_1\right) - \mathcal{Z}_2\mathcal{Z}_3 I_0(\mathcal{Z}_4)\right]. \quad (46)$$

Special Case: The closed-form expression for the OP of U_2 for Rayleigh fading channel can be obtained by setting $s=0$ in (35), as given by

$$\overline{\mathrm{P}}_{U_2} = 1 - \frac{\sigma_{U_1}^2 e^{-\frac{\widetilde{\theta}\xi}{\sigma_{U_1}^2} - \widetilde{k}\overline{\theta}\xi + \frac{1}{4\mathcal{D}\sigma_S^4}}}{\sigma_S^2(\sigma_{U_1}^2 + \rho_2\widetilde{\theta}\sigma_{U_2}^2)}\sqrt{\frac{\pi}{\mathcal{D}}}Q\left(\frac{1}{\sigma_S^2}\sqrt{\frac{2}{\mathcal{D}}}\right), \quad (47)$$

where $\widetilde{k} = \frac{\sigma_{U_1}^2 + \widetilde{\theta}\rho_2\sigma_{U_2}^2}{\sigma_{U_1}^2\sigma_{U_2}^2}$, $\mathcal{D} = \widetilde{k}\overline{\theta}\eta^2\rho + \frac{\widetilde{\theta}\eta^2\rho}{\sigma_{U_1}^2}$, and $\overline{\theta} = \frac{\lambda_{22}}{\rho_2}$. The OP expressions for both UL and DL users are derived under the impact of radar interference and inter-user interference. Furthermore, in Section VI, through numerical results, we discuss and illustrate in detail the impact of these interferences on the outage performance in UL and DL scenarios.

B. Ergodic Rate Analysis

In this subsection, we investigate another performance metric of CUs in terms of the average achievable rate. We derive the approximate expressions of the ergodic rate for the near and far CUs in the DL and UL scenarios over Rician fading channels using Jensen's inequality and the first-order Taylor series approximation [31], [32]. The ergodic rate is defined as the average achievable rate, which is used to characterize the performance of the user's rate depending on the channel

---

$$\mathcal{F}_1 = 1 - \sum_{n_2=0}^{\infty}\frac{(-1)^{n_2}}{\Gamma(n_2+2)}e^{-\frac{s^2}{\sigma_{U_2}^2}}L_{n_2}^0\left(\frac{s^2}{\sigma_{U_2}^2}\right)\left(\frac{\lambda_{22}}{\rho_2\sigma_{U_2}^2}\right)^{n_2+1}\left(\xi^{n_2+1} + \eta^2\rho\xi^{n_2}(n_2+1)\mathbb{E}[W^2]\right), \quad (36)$$

where $\mathbb{E}[W^2] = 2\sigma_S^2\exp\left(-\frac{s^2}{\sigma_S^2}\right){}_1F_1\left(3;1;\frac{s^2}{\sigma_S^2}\right)$.

$$\mathcal{F}_2 = \mathcal{K}_1\xi^{n_1+1} + \mathcal{K}_1(n_1+1)\rho\eta^2\xi^{n_1}\mathbb{E}[W^2] - \mathcal{K}_1\mathcal{K}_2\xi^{n_1+n_3+2} - \mathcal{K}_1\mathcal{K}_2\xi^{n_1+n_3+1}(n_1+n_3+2)\eta^2\rho\mathbb{E}[W^2], \quad (37)$$

where $\mathcal{K}_1 = \sum_{n_1=0}^{\infty}\frac{(-1)^{n_1}}{\Gamma(n_1+2)}e^{-\frac{s^2}{\sigma_{U_1}^2}}L_{n_1}^0\left(\frac{s^2}{\sigma_{U_1}^2}\right)\left(\frac{\lambda_{11}}{\rho_1\sigma_{U_1}^2}\right)^{n_1+1}$, $\mathcal{K}_2 = \sum_{n_3=0}^{\infty}\frac{(-1)^{n_3}}{\Gamma(n_3+2)}e^{-\frac{s^2}{\sigma_{U_2}^2}}L_{n_3}^0\left(\frac{s^2}{\sigma_{U_2}^2}\right)\left(\frac{\lambda_{11}}{\rho_1\sigma_{U_2}^2}\right)^{n_3+1}$.

$$\mathcal{F}_3 = (n_1+1)\rho_2(s^2+\sigma_{U_2}^2)\mathcal{K}_1\left\{(\xi^{n_1} + n_1\eta^2\rho\xi^{n_1-1}\mathbb{E}[W^2]) - \mathcal{K}_3\left(\xi^{n_1+n_4+1} + \xi^{n_1+n_4}(n_1+n_4+1)\eta^2\rho\mathbb{E}[W^2]\right)\right\}, \quad (38)$$

where $\mathcal{K}_3 = \sum_{n_4=0}^{\infty}\frac{(-1)^{n_4}}{\Gamma(n_4+2)}e^{-\frac{s^2}{\sigma_{U_2}^2}}L_{n_4}^0\left(\frac{s^2}{\sigma_{U_2}^2}\right)\left(\frac{\lambda_{22}}{\rho_2\sigma_{U_2}^2}\right)^{n_4+1}$.

$$\mathcal{F}_4 = \mathcal{K}_4\sum_{n_5=0}^{\infty}\left(\frac{s}{\sigma_{U_2}^2}\right)^{2n_5+1}\left(\frac{\lambda_{22}}{\rho_2}\right)^{n_5+1}\frac{\xi^{n_1+n_5+1}}{n_5!\Gamma(n_5+2)}\left\{1 - \left(\frac{\lambda_{22}\eta^2\rho}{\rho_2\sigma_{U_2}^2} + \frac{(n_1+n_5+1)\eta^2\rho}{\xi}\right)\mathbb{E}[W^2] - \frac{(n_1+n_5+1)\eta^4\rho^2\lambda_{22}}{\rho_2\xi\sigma_{U_2}^2}\mathbb{E}[W^4]\right\}, \quad (39)$$

$$\mathcal{F}_5 = \frac{\mathcal{K}_4}{s}\sum_{n_6=0}^{\infty}\left(\frac{s}{\sigma_{U_2}^2}\right)^{2n_6}\left(\frac{\lambda_{22}}{\rho_2}\right)^{n_6+1}\frac{\xi^{n_1+n_6+1}}{(n_6!)^2}\left\{1 + \left(\frac{\frac{(n_1+n_6+1)}{\xi} - \lambda_{22}\eta^2\rho}{\rho_2\sigma_{U_2}^2}\right)\mathbb{E}[W^2] - \frac{(n_1+n_6+1)\eta^4\rho^2\lambda_{22}}{\rho_2\xi\sigma_{U_2}^2}\mathbb{E}[W^4]\right\}, \quad (40)$$

where $\mathcal{K}_4 = s\rho_2\mathcal{K}_1(n_1+1)\exp\left(-\frac{s^2 + \frac{\lambda_{22}\xi}{\rho_2}}{\sigma_{U_2}^2}\right)$, $\mathbb{E}[W^4] = 4!\,\sigma_S^4\exp\left(-\frac{s^2}{\sigma_S^2}\right){}_1F_1\left(5;1;\frac{s^2}{\sigma_S^2}\right)$.

$$\mathcal{I}_1 = 1 - \underbrace{\sum_{n_2=0}^{\infty}\frac{(-1)^{n_2}}{\Gamma(n_2+2)}e^{-\frac{s^2}{\sigma_{U_2}^2}}L_{n_2}^0\left(\frac{s^2}{\sigma_{U_2}^2}\right)\left(\frac{\mathcal{B}}{\sigma_{U_2}^2}\right)^{n_2+1}}_{\mathcal{M}_1} - \underbrace{\sum_{n_1=0}^{\infty}\frac{(-1)^{n_1}}{\Gamma(n_1+2)}e^{-\frac{s^2}{\sigma_{U_1}^2}}L_{n_1}^0\left(\frac{s^2}{\sigma_{U_1}^2}\right)\left(\frac{\lambda_{11}(\xi+w\eta^2\rho)}{\rho_1}\right)^{n_1+1}}_{\mathcal{M}_2}$$
$$\left[\underbrace{Q_1(\omega_1,\omega_2)}_{\mathcal{M}_3} + \underbrace{\frac{(n_1+1)\rho_2}{(\xi+w\eta^2\rho)}}_{\mathcal{M}_4}\left(\underbrace{(s^2+\sigma_{U_2}^2)Q_1(\omega_1,\omega_2)}_{\mathcal{M}_5} + \underbrace{\sqrt{\mathcal{B}}e^{-\frac{s^2+\mathcal{B}}{\sigma_{U_2}^2}}\left(sI_1(\omega_3) + \sqrt{\mathcal{B}}I_0(\omega_3)\right)}_{\mathcal{M}_6}\right)\right]. \quad (44)$$

conditions of the CUs. Thus, the ergodic rate of the user is given by

$$\overline{\mathrm{R}}_{\kappa} = \mathbb{E}\left[\log\left(1+\Upsilon\right)\right], \tag{48}$$

where $\kappa \in \{D_1, D_2, U_1, U_2\}$ denotes the rate achieved by the users and $\Upsilon \in \{\gamma_{1,D_1}, \gamma_{2,D_2}, \gamma_{1,U_1}, \gamma_{2,U_2}\}$ denotes the corresponding SINRs as given in (5)-(8). The ergodic rate in (48) can be simplified using [33, (16)] as

$$\overline{\mathrm{R}}_{\kappa}=\int_0^{\infty}\log(1+\Upsilon)p_{\Upsilon}(r)\,\mathrm{d}r = \frac{1}{\ln 2}\int_0^{\infty}\frac{1-F_{\Upsilon}(r)}{1+r}\,\mathrm{d}r\,. \tag{49}$$

1) Downlink Transmission: The ergodic rate of transmission from the BS to the near user D_1 can be obtained by substituting $\kappa = D_1$ and $\Upsilon = \gamma_{1,D_1}$ in (48), where γ_{1,D_1} is given in (5). The CDF $F_{\Upsilon}(r)$ can be expressed as

$$\begin{aligned}F_{\Upsilon}(r) &= \Pr[\Upsilon \le r] = \Pr[\gamma_{1,D_1} \le r]\\ &= \Pr\left[|h_1|^2 \le \frac{r(\zeta_{D_1}^2 P + |f_{11}|^2P_1 + |f_{21}|^2P_2 + \sigma^2)}{\alpha P}\right]. \end{aligned}\tag{50}$$

Therefore, $F_{\Upsilon}(r)$ in (50) can be written as

$$F_{\Upsilon}(r)=\int_0^{\infty}p_{|f_{21}|^2}(w)\int_0^{\infty}p_{|f_{11}|^2}(v)\int_0^{\mathcal{U}}p_{|h_1|^2}(u)\,\mathrm{d}u\,\mathrm{d}v\,\mathrm{d}w\,, \tag{51}$$

where $\mathcal{U} = r(P\zeta_{D_1}^2 + vP_1 + wP_2 + \sigma^2)(\alpha P)^{-1}$. On solving the integrals in (51) similar to the steps discussed in the proof of Theorem 1, we get

$$F_{\Upsilon}(r)=\sum_{k=0}^{\infty} e^{-\frac{s^2}{\sigma_{D_1}^2}}\frac{(-1)^k}{\Gamma(k+2)}L_k^0\left(\frac{s^2}{\sigma_{D_1}^2}\right)\left(\frac{r}{\alpha\rho\sigma_{D_1}^2}\right)^{k+1}\mathcal{T}, \tag{52}$$

where $\mathcal{T} = t_1 + t_2 + t_3$, with $t_1 = (\rho\zeta_{D_1}^2 + 1)^{k+1}$, $t_2 = (k+1)(\rho\zeta_{D_1}^2+1)^k\left[\rho_1(s^2+\sigma_{11}^2) + \rho_2(s^2+\sigma_{21}^2)\right]$, $t_3 = \rho_1\rho_2 k(k+1)(\rho\zeta_{D_1}^2+1)^{k-1}(s^2+\sigma_{11}^2)(s^2+\sigma_{21}^2)$. Upon substituting (52) in (49), we observe that it is mathematically intractable to obtain the closed-form expression of the ergodic rate for D_1 over a Rician fading channel. Thus, we use Jensen's inequality, a fundamental upper bound on the ergodic rate of the CU and the first-order Taylor series approximation as given in [31] and [32] to obtain the approximate achievable rate of D_1 as

$$\begin{aligned}&\mathbb{E}[\log(1+\gamma_{1,D_1})] \le \log(1+\mathbb{E}[\gamma_{1,D_1}])\\ &\approx \log\left(1 + \frac{\mathbb{E}[\alpha|h_1|^2P]}{\mathbb{E}[\zeta_{D_1}^2P + |f_{11}|^2P_1 + |f_{21}|^2P_2 + \sigma^2]}\right).\end{aligned}\tag{53}$$

After taking expectation, the ergodic rate $\overline{\mathrm{R}}_{D_1}$ simplifies to

$$\overline{\mathrm{R}}_{D_1}\approx\log\left(1 + \frac{\alpha\rho(s^2+\sigma_{D_1}^2)}{\zeta_{D_1}^2\rho + (s^2+\sigma_{11}^2)\rho_1 + (s^2+\sigma_{21}^2)\rho_2 + 1}\right). \tag{54}$$

Special Case: Substituting $s = 0$ in (1), the PDF of $|Y|^2$ follows central chi-square with 2 DoF and further. Using this fact in (51) and after mathematical manipulations, (51) can be simplified to

$$F_{\Upsilon}(r) = 1 - \frac{(\alpha\rho\sigma_{D_1}^2)^2\exp\left[-\frac{r(\rho\zeta_{D_1}^2+1)}{\alpha\rho\sigma_{D_1}^2}\right]}{(\alpha\rho\sigma_{D_1}^2 + r\rho_2\sigma_{21}^2)(\alpha\rho\sigma_{D_1}^2 + r\rho_1\sigma_{11}^2)}. \tag{55}$$

To derive $\overline{\mathrm{R}}_{D_1}$ using (55), we assume $\delta = \frac{\alpha\rho\sigma_{D_1}^2}{\rho_2\sigma_{21}^2}$, $\lambda = \frac{\alpha\rho\sigma_{D_1}^2}{\rho_1\sigma_{11}^2}$, and $\mu = \frac{\rho\zeta_{D_1}^2+1}{\alpha\rho\sigma_{D_1}^2}$. Substituting the expressions of δ, λ, and μ in (55), and by plugging the resultant expression into (49), $\overline{\mathrm{R}}_{D_1}$ becomes

$$\overline{\mathrm{R}}_{D_1} = \frac{1}{\ln 2}\int_0^{\infty}\frac{\delta\lambda}{(\delta+r)(\lambda+r)(1+r)}e^{-r\mu}\,\mathrm{d}r\,. \tag{56}$$

We will now evaluate (56) for the following two cases:
i) δ and λ are equal to 1: By applying [29, (3.353.2)], the closed-form expression for (56) can be obtained as

$$\overline{\mathrm{R}}_{D_1} = \frac{1-\mu-\mu^2 e^{\mu}\,\mathrm{Ei}(-\mu)}{2\ln 2}. \tag{57}$$

ii) δ and λ are not equal to 1: $\overline{\mathrm{R}}_{D_1}$ in (56) can be evaluated by utilizing the partial fraction decomposition method. Further, the closed-form expression after applying [29, (3.352.4)] can be obtained as

$$\begin{aligned}\overline{\mathrm{R}}_{D_1} = \frac{\delta\lambda}{\ln 2}\Bigg(&-\frac{e^{\delta\mu}\,\mathrm{Ei}(-\delta\mu)}{(\lambda-\delta)(1-\delta)} - \frac{e^{\lambda\mu}\,\mathrm{Ei}(-\lambda\mu)}{(\delta-\lambda)(1-\lambda)}\\ &-\frac{e^{\mu}\,\mathrm{Ei}(-\mu)}{(\lambda-1)(\delta-1)}\Bigg).\end{aligned}\tag{58}$$

The ergodic rate of transmission from the BS to the far user D_2 can be obtained by substituting $\kappa = D_2$ and $\Upsilon = \gamma_{2,D_2}$ in (48), where γ_{2,D_2} is given in (6). The CDF of Υ by following the similar approach as given in (50) and (51), can be expressed as

$$F_{\Upsilon}(r) = \int_0^{\infty}p_{|f_{22}|^2}(w)\int_0^{\infty}p_{|f_{12}|^2}(v)\int_0^{\mathcal{V}}p_{|h_2|^2}(u)\,\mathrm{d}u\,\mathrm{d}v\,\mathrm{d}w\,, \tag{59}$$

where $\mathcal{V} = r(P\zeta_{D_2}^2 + vP_1 + wP_2 + \sigma^2)((1-\alpha(1+r))P)^{-1}$. On solving these integrals in (59), the closed-form expression is obtained as

$$\begin{aligned}F_{\Upsilon}(r) = &\sum_{k=0}^{\infty} e^{-\frac{s^2}{\sigma_{D_2}^2}}\frac{(-1)^k}{\Gamma(k+2)}L_k^0\left(\frac{s^2}{\sigma_{D_2}^2}\right)\widetilde{\mathcal{T}}\\ &\times\left(\frac{r}{(1-\alpha-r\alpha)\rho\sigma_{D_2}^2}\right)^{k+1}\left[\varepsilon(r) - \varepsilon\left(r - \frac{1-\alpha}{\alpha}\right)\right],\end{aligned}\tag{60}$$

where $\widetilde{\mathcal{T}} = \widetilde{t}_1 + \widetilde{t}_2 + \widetilde{t}_3$, with $\widetilde{t}_1 = (\rho\zeta_{D_1}^2 + 1)^{k+1}$, $\widetilde{t}_2 = (k+1)(\rho\zeta_{D_1}^2+1)^k\left[\rho_1(s^2+\sigma_{11}^2) + \rho_2(s^2+\sigma_{21}^2)\right]$, $\widetilde{t}_3 = \rho_1\rho_2 k(k+1)(\rho\zeta_{D_1}^2+1)^{k-1}(s^2+\sigma_{11}^2)(s^2+\sigma_{21}^2)$, and $\varepsilon(\cdot)$ represents the unit step function. By applying Jensen's inequality and the first-order Taylor series approximation as discussed and applied in (53), the approximate expression of the ergodic rate for D_2 can be expressed as (61), as shown at the bottom of the next page.

Remark 3: The average achievable rate in the DL scenario is sensitive to the variance of the interference channel caused by the BS signal reflected via the target and by co-channel signals from UL users (i.e., transmit SNRs), and it is inversely proportional to these parameters.

Special Case: By substituting $s = 0$ in (59), $F_{\Upsilon}(r)$ can be expressed as

$$F_{\Upsilon}(r) = 1 - \frac{((1-\alpha-r\alpha)\rho\sigma_{D_2}^2)^2}{(1-\alpha-r\alpha)\rho\sigma_{D_2}^2 + r\rho_2\sigma_{22}^2}e^{-\frac{r(\rho\zeta_{D_2}^2+1)}{\alpha\rho\sigma_{D_2}^2}}$$

$$\times \frac{1}{(1-\alpha-r\alpha)\rho\sigma_{D_2}^2+r\rho_1\sigma_{12}^2}\left[\varepsilon(r)-\varepsilon\left(r-\frac{1-\alpha}{\alpha}\right)\right]. \tag{62}$$

Substituting (62) in (49), we numerically evaluate the ergodic rate $\overline{\mathrm{R}}_{D_2}$, the results of which are discussed in Section VI.

2) Uplink Transmission: In the presence of a target, the ergodic rate achieved by the far user U_2 in the UL transmission phase can be obtained by substituting $\kappa = U_2$ and $\Upsilon = \gamma_{2,U_2}$ in (48), where γ_{2,U_2} is given in (8). From (8) and by following the similar approach as discussed in Section III-B.1, the CDF of Υ can be expressed as

$$F_\Upsilon(r) = \int_0^\infty p_{|h|^2}(v)\int_0^{\mathcal{X}} p_{|g_2|^2}(u)\,\mathrm{d}u\,\mathrm{d}v\,. \tag{63}$$

where $\mathcal{X} = r(P_1\zeta_{U_1}^2+P_2\zeta_{U_2}^2+P\eta^2v+\sigma^2)P_2^{-1}$. On solving the integrals in (63), we get

$$F_\Upsilon(r) = \sum_{k=0}^{\infty} e^{-\frac{s^2}{\sigma_{U_2}^2}}\frac{(-1)^k}{\Gamma(k+2)}L_k^0\left(\frac{s^2}{\sigma_{U_2}^2}\right)\left(\frac{r}{\rho_2\sigma_{U_2}^2}\right)^{k+1}\mathcal{I}, \tag{64}$$

where $\mathcal{I} = i_1+i_2$, with $i_1 = \xi^{k+1}$ and $i_2 = (k+1)\xi^k\eta^2\rho(s^4+4s^2\sigma_S^2+2\sigma_S^4)$. The approximate ergodic rate $\overline{\mathrm{R}}_{U_2}$ of user U_2 after following a similar approach as in (53) can be written as

$$\overline{\mathrm{R}}_{U_2} \approx \log\left(1+\frac{\rho_2(s^2+\sigma_{U_2}^2)}{\rho_2\zeta_{U_2}^2+\rho_1\zeta_{U_1}^2+\eta^2\rho(s^2+4s^2\sigma_S^2+2\sigma_S^4)+1}\right). \tag{65}$$

Special Case: For the Rayleigh fading case, where $s = 0$, on solving the integration in (63) by utilizing [29, (3.322.2)], we obtain the CDF expression as given by

$$F_\Upsilon(r) = 1-\exp\left[-\frac{r\,\xi}{\rho_2\sigma_{U_2}^2}+\frac{\rho_2\sigma_{U_2}^2}{4r\rho\eta^2\sigma_S^4}\right] \times \frac{1}{2\sigma_S^2}\sqrt{\frac{\pi\rho_2\sigma_{U_2}^2}{r\rho\eta^2}}\operatorname{erfc}\left(\frac{1}{2\sigma_S^2}\sqrt{\frac{\rho_2\sigma_{U_2}^2}{r\rho\eta^2}}\right). \tag{66}$$

On substituting (66) into (49) and utilizing the Gauss-Laguerre quadrature method to obtain the ergodic rate $\overline{\mathrm{R}}_{U_2}$, we get

$$\overline{\mathrm{R}}_{U_2} = \sum_{q=1}^{n}\psi_q\exp\left[-\frac{b_q\,\xi}{\rho_2\,\sigma_{U_2}^2}+\frac{\rho_2\,\sigma_{U_2}^2}{4b_q\rho\eta^2\sigma_S^4}+b_q\right] \times \frac{1}{2\sigma_S^2}\sqrt{\frac{\pi\rho_2\sigma_{U_2}^2}{b_q\rho\eta^2}}\operatorname{erfc}\left(\frac{1}{2\sigma_S^2}\sqrt{\frac{\rho_2\sigma_{U_2}^2}{b_q\rho\eta^2}}\right), \tag{67}$$

where b_q represents the nth roots of the Laguerre polynomial $L_n(b)$ [29], and ψ_q denotes the weights which are given by $\psi_q = \frac{b_q}{(n+1)^2[L_{n+1}(b_q)]^2}$. Furthermore, in the UL scenario, since the target echo is received at the BS, it is more meaningful to derive the ergodic rates in the absence of a target, which provides some insights about the achievable rate performance. However, in the DL scenario, the analysis in the absence of the sensing-to-communication interference channels is straightforward from (55) by substituting $\zeta_{D_1}^2 = 0$. Thus, for the UL case, when the target is absent, i.e., $\eta = 0$, $\zeta_{U_1}^2 = 0$, $\zeta_{U_2}^2 = 0$, the ergodic rate is given by $\widetilde{\mathrm{R}}_{U_2} = \mathbb{E}\left[\log\left(1+\frac{P_2|g_2|^2}{\sigma^2}\right)\right]$. With this, the CDF becomes $F_\Upsilon(r) = 1-\exp\left[-\frac{r}{\rho_2\sigma_{U_2}^2}\right]$, substituting into (49) and solving the integral using [29, (3.352.4)], the ergodic rate expression becomes

$$\widetilde{\mathrm{R}}_{U_2} = -\frac{1}{\ln 2}\exp\left[\frac{1}{\rho_2\sigma_{U_2}^2}\right]\mathrm{Ei}\left(-\frac{1}{\rho_2\sigma_{U_2}^2}\right). \tag{68}$$

In the presence of a target, the ergodic rate achieved by the near user U_1 in the UL transmission phase can be obtained by substituting $\kappa = U_1$ and $\Upsilon = \gamma_{1,U_1}$ in (48), where γ_{1,U_1} is given in (7). From (7) and by following the similar approach as discussed in Section III-B.1, the CDF of Υ is expressed as

$$F_\Upsilon(r) = \sum_{k=0}^{\infty} e^{-\frac{s^2}{\sigma_{U_1}^2}}\frac{(-1)^k}{\Gamma(k+2)}L_k^0\left(\frac{s^2}{\sigma_{U_1}^2}\right)\left(\frac{r}{\rho_1\sigma_{U_1}^2}\right)^{k+1}\widetilde{\mathcal{I}}, \tag{69}$$

where $\widetilde{\mathcal{I}} = \widetilde{i}_1+\widetilde{i}_2+\widetilde{i}_3$, with $\widetilde{i}_1 = \xi^{k+1}$, $\widetilde{i}_2 = (k+1)\xi^k\left[\eta^2\rho(s^4+4s^2\sigma_S^2+2\sigma_S^4)+\rho_2(s^2+\sigma_{U_2}^2)\right]$, and $\widetilde{i}_3 = \eta^2\rho\rho_2k(k+1)\xi^{k-1}(s^4+4s^2\sigma_S^2+2\sigma_S^4)(s^2+\sigma_{U_2}^2)$. The approximate ergodic rate $\overline{\mathrm{R}}_{U_1}$ of the near user U_1 after following a similar approach as in (53) can be obtained as

$$\overline{\mathrm{R}}_{U_1} \approx \log\left(1+\frac{\rho_1(s^2+\sigma_{U_1}^2)}{\mathcal{L}}\right), \tag{70}$$

where $\mathcal{L} = (s^2+\sigma_{U_2}^2+\zeta_{U_2}^2)\rho_2+\zeta_{U_1}^2\rho_1+\eta^2\rho(s^4+4s^2\sigma_S^2+2\sigma_S^4)+1$.

Remark 4: The ergodic rate in the UL scenario is inversely proportional to the quadratic variance of the effective cascaded channel (target echo), the downlink transmit SNR of the BS, and the target scattering coefficient.

Special Case: For the Rayleigh fading channel, substituting $s = 0$ in (63), the CDF of Υ can be written as

$$F_\Upsilon(r) = 1-\frac{\rho_1\sigma_{U_1}^2}{2\sigma_S^2(\rho_1\sigma_{U_1}^2+r\rho_2\sigma_{U_2}^2)}\sqrt{\frac{\pi\rho_1\sigma_{U_1}^2}{r\rho\eta^2}} \times\exp\left[-\frac{r\,\xi}{\rho_1\sigma_{U_1}^2}+\frac{\rho_1\sigma_{U_1}^2}{4r\rho\eta^2\sigma_S^4}\right]\operatorname{erfc}\left(\frac{1}{2\sigma_S^2}\sqrt{\frac{\rho_2\sigma_{U_2}^2}{r\rho\eta^2}}\right). \tag{71}$$

Upon substituting (71) into (49) and utilizing the Gauss-Laguerre quadrature method, the ergodic rate $\overline{\mathrm{R}}_{U_1}$ in the presence of the target can be obtained as

$$\overline{\mathrm{R}}_{U_1} = \sum_{q=1}^{n}\psi_q\exp\left[-\frac{b_q\,\xi}{\rho_1\sigma_{U_1}^2}+\frac{\rho_1\sigma_{U_1}^2}{4b_q\rho\eta^2\sigma_S^4}+b_q\right]$$

$$\overline{\mathrm{R}}_{D_2} \approx \log\left(1+\frac{(1-\alpha)\rho(s^2+\sigma_{D_2}^2)}{((\alpha(s^2+\sigma_{D_2}^2)+\zeta_{D_2}^2)\rho+(s^2+\sigma_{12}^2)\rho_1+(s^2+\sigma_{22}^2)\rho_2+1}\right). \tag{61}$$

$$\times \frac{\rho_1 \sigma_{U_1}^2 \sqrt{\frac{\pi \rho_1 \sigma_{U_1}^2}{b_q \rho \eta^2}}}{2\sigma_S^2(\rho_1 \sigma_{U_1}^2 + b_q \rho_2 \sigma_{U_2}^2)} \mathrm{erfc}\left(\frac{1}{2\sigma_S^2}\sqrt{\frac{\rho_2 \sigma_{U_2}^2}{b_q \rho \eta^2}}\right). \quad (72)$$

As discussed for the case of the far user in the UL scenario over the Rayleigh fading channel, we also discuss the achievable ergodic rate for the near user when the target is absent. The ergodic rate can be expressed as $\widetilde{\mathrm{R}}_{U_1} = \mathbb{E}\left[\log\left(1 + \frac{|g_1|^2 P_1}{|g_2|^2 P_2 + \sigma^2}\right)\right]$. The CDF of $\Upsilon = \frac{|g_1|^2 P_1}{|g_2|^2 P_2 + \sigma^2}$ can be obtained as $F_\Upsilon(r) = 1 - \frac{\rho_1 \sigma_{U_1}^2}{\rho_1 \sigma_{U_1}^2 + r \rho_2 \sigma_{U_2}^2} \exp\left[-\frac{r}{\rho_1 \sigma_{U_1}^2}\right]$. Further, substituting $\tau = \frac{\rho_1 \sigma_{U_1}^2}{\rho_2 \sigma_{U_2}^2}$ and $\varphi = \frac{1}{\rho_1 \sigma_{U_1}^2}$ in the obtained CDF and plugging the expression into (49), the ergodic rate can be written as $\widetilde{\mathrm{R}}_{U_1} = \frac{1}{\ln 2}\int_0^\infty \frac{\tau}{(\tau+r)(1+r)} e^{-r\varphi}\, \mathrm{d}r$. For $\tau = 1$ and using [29, (3.353.3)], the final expression is given by

$$\widetilde{\mathrm{R}}_{U_1} = \frac{\varphi\, e^{\varphi}\, \mathrm{Ei}(-\varphi) + 1}{\ln 2}. \quad (73)$$

For the case of $\tau \neq 1$, with the help of partial fraction decomposition and by utilizing [29, (3.352.4)], the ergodic rate simplifies to

$$\widetilde{\mathrm{R}}_{U_1} = \frac{\tau}{(\tau - 1)\ln 2}\left[-e^{\varphi}\, \mathrm{Ei}(-\varphi) - e^{\tau\varphi}\, \mathrm{Ei}(-\tau\varphi)\right]. \quad (74)$$

IV. Sensing Performance Analysis

In this section, we evaluate the sensing performance of the NOMA-assisted ISAC system by focusing on the target detection problem. In Section III, we derived the performance metrics of CUs. Here, we gain insights by observing the performance tradeoff between communication and sensing functionalities by deriving and analyzing the probability of detection (P_D) and false alarm (P_F). In our system, the BS receives signals from UL CUs and the sensing echo. As a result, during the decoding of the UL user's information signal, the target echo acts as an interference, and during the target detection, the UL users' signals act as interference. Therefore, the detection of a single static target can be formulated as a binary hypothesis testing problem in the context of an ISAC system. Specifically, $\mathcal{H}_0$ denotes the null hypothesis, representing the presence of noise and interference from UL users without a target, while $\mathcal{H}_1$ denotes the alternative hypothesis, indicating the presence of a target along with noise and interference from UL CUs. The received signals at the BS under these two hypotheses are given by

$$\mathcal{H}_0 : r_{BS} = \underbrace{(g_1 + \beta_{U_1})s_1}_{\text{UL near CU interference}} + \underbrace{(g_2 + \beta_{U_2})s_2}_{\text{UL far CU interference}} + \underbrace{z}_{\text{AWGN}}, \quad (75)$$

$$\mathcal{H}_1 : r_{BS} = \underbrace{\eta h x}_{\text{Target echo}} + (g_1 + \beta_{U_1})s_1 + (g_2 + \beta_{U_2})s_2 + z. \quad (76)$$

We assume that the BS has perfect knowledge of the channel state information (CSI), signal power, and noise variance. Further, we use the Neyman-Pearson (NP) criterion to distinguish between the hypotheses $\mathcal{H}_0$ and $\mathcal{H}_1$. The NP detector [34] is expressed by following condition

$$\Lambda(r_{BS}) = \frac{p(r_{BS}|\mathcal{H}_1)}{p(r_{BS}|\mathcal{H}_0)} \underset{\mathcal{H}_0}{\overset{\mathcal{H}_1}{\gtrless}} \varrho, \quad (77)$$

where ϱ is a certain threshold, $p(r_{BS}|\mathcal{H}_1)$ and $p(r_{BS}|\mathcal{H}_0)$ denote the conditional PDFs of r_{BS} given $\mathcal{H}_1$ and $\mathcal{H}_0$, respectively, and $\Lambda(r_{BS})$ represents the likelihood ratio. Since r_{BS} is a complex Gaussian distributed RV under both $\mathcal{H}_0$ and $\mathcal{H}_1$, the conditional PDFs can be respectively expressed as

$$p(r_{BS}|\mathcal{H}_0) = \frac{1}{\pi \mathrm{Var}(\mathcal{H}_0)} \exp\left(-\frac{|r_{BS}|^2}{\mathrm{Var}(\mathcal{H}_0)}\right), \quad (78)$$

$$p(r_{BS}|\mathcal{H}_1) = \frac{1}{\pi \mathrm{Var}(\mathcal{H}_1)} \exp\left(-\frac{|r_{BS}|^2}{\mathrm{Var}(\mathcal{H}_1)}\right), \quad (79)$$

where $\mathrm{Var}(\mathcal{H}_0) = (\sigma_{U_1}^2 + \zeta_{U_1}^2)P_1 + (\sigma_{U_2}^2 + \zeta_{U_2}^2)P_2 + \sigma^2$ and $\mathrm{Var}(\mathcal{H}_1) = (\sigma_{U_1}^2 + \zeta_{U_1}^2)P_1 + (\sigma_{U_2}^2 + \zeta_{U_2}^2)P_2 + \eta^2 P \mathrm{Var}(h) + \sigma^2$, denote the variances of r_{BS} under $\mathcal{H}_0$ and $\mathcal{H}_1$, respectively, with $\mathrm{Var}(h) = 8s^6\sigma_S^2 + 52s^4\sigma_S^4 + 80s^2\sigma_S^6 + 20\sigma_S^4$. The NP detector in (77) decides $\mathcal{H}_1$ if the below condition is satisfied

$$|r_{BS}|^2 > \bar{\varrho}, \quad (80)$$

where

$$\bar{\varrho} = \frac{\mathrm{Var}(\mathcal{H}_0)\mathrm{Var}(\mathcal{H}_1)}{\mathrm{Var}(\mathcal{H}_1) - \mathrm{Var}(\mathcal{H}_0)} \ln\left(\frac{\mathrm{Var}(\mathcal{H}_1)}{\mathrm{Var}(\mathcal{H}_0)}\varrho\right).$$

For the detector in (77), the probability of false alarm $P_F = \Pr(|r_{BS}|^2 > \bar{\varrho}|\mathcal{H}_0)$ and the probability of detection $P_D = \Pr(|r_{BS}|^2 > \bar{\varrho}|\mathcal{H}_1)$. The received signal power at the BS, $|r_{BS}|^2$, follows a non-central chi-square distribution having 3 DoF under $\mathcal{H}_0$ and 4 DoF under $\mathcal{H}_1$ [35]. Therefore, the P_F can be derived by using the CDF of a non-central chi-square distribution with 3 DoF, as given by

$$P_F = 1 - \Pr(|r_{BS}|^2 < \bar{\varrho}|\mathcal{H}_0) = Q_{\frac{3}{2}}\left(\sqrt{\frac{\mathcal{S}_1}{\sigma^2}}, \sqrt{\frac{2\bar{\varrho}}{\sigma^2}}\right), \quad (81)$$

where $\mathcal{S}_1 = 2((|g_1|^2 + \zeta_{U_1}^2)P_1 + (|g_2|^2 + \zeta_{U_2}^2)P_2)$. Further, the probability of detection can be derived by again using the CDF of a non-central chi-square distribution with 4 DoF, given as

$$P_D = 1 - \Pr(|r_{BS}|^2 < \bar{\varrho}|\mathcal{H}_1) = Q_2\left(\sqrt{\frac{\mathcal{S}_2}{\sigma^2}}, \sqrt{\frac{2\bar{\varrho}}{\sigma^2}}\right), \quad (82)$$

where $\mathcal{S}_2 = 2((|g_1|^2 + \zeta_{U_1}^2)P_1 + (|g_2|^2 + \zeta_{U_2}^2)P_2 + \eta^2|h|^2 P)$.

Remark 5: In (82), P_D is a function of the UL CUs transmit powers P_1 and P_2, and the DL transmit power P, thereby highlighting the trade-off between target detection accuracy and CU performance in the proposed NOMA-assisted ISAC system.

V. Uplink Power Optimization

In this section, we design a communication-centric max-min power allocation optimization problem while also ensuring a minimum constraint on the radar target detection. This is mainly to integrate the target sensing capability into the communication-centric design, aiming to enhance fairness and ensure consistent quality-of-service for UL users. Thus, the trade-off between communication and sensing functionalities exists as the target echo acts as an interference to UL CUs at the BS and vice versa. In practice, in the UL scenario, the CUs transmit with full power to maximize their data rate. As a result, the UL CUs have different achievable rates. Assuming that the instantaneous CSI is known at the BS, the instantaneous rates of the two UL users U_1 and U_2 are respectively given by

$$\mathrm{R}_1 = \log\left(1+\frac{|g_1|^2\rho_1}{(|g_2|^2+\zeta_{U_2}^2)\rho_2+\zeta_{U_1}^2\rho_1+\eta^2|h|^2\rho+1}\right), \quad (83)$$

$$\mathrm{R}_2 = \log\left(1+\frac{|g_2|^2\rho_2}{\zeta_{U_1}^2\rho_1+\zeta_{U_2}^2\rho_2+\eta^2|h|^2\rho+1}\right). \quad (84)$$

A. Max-Min Power Allocation

In this subsection, we investigate the performance of the max-min power allocation strategy, such that the UL CUs achieve an optimal rate. Given the exponential growth in the number of connected devices, improving the achievable rate by increasing the transmit power is not a suitable solution due to economic and environmental concerns. It also increases interference to the DL CUs (co-channel) and at the BS affects the target detection, thus, degrading the overall system performance. Therefore, the motivation for choosing the max-min scheme is to create fairness in the achievable rate among the UL CUs while maintaining overall system performance. This scheme aims to maximize the performance of the unfortunate user, thereby ensuring user fairness. This can be achieved by maximizing the minimum rate, which, in turn, also implies maximization of the minimum of the two SINRs γ_{1,U_1} and γ_{2,U_2} as given in (7) and (8), respectively.

This problem formulation can be achieved by using the epigraph form of optimization such that the SINRs γ_{1,U_1} and γ_{2,U_2} are greater than γ_{aux}, where γ_{aux} denotes an auxiliary variable. Thus, the modified objective function aims to maximize the auxiliary variable over the transmit powers P_1 and P_2 of users U_1 and U_2, respectively. The max-min power allocation optimization problem can be formulated as

$$\begin{aligned} \max_{P_1,P_2} \quad & \gamma_{\text{aux}} \\ \text{s.t.} \quad & \gamma_{1,U_1}, \gamma_{2,U_2} \geq \gamma_{\text{aux}} \\ & 0 \leq P_1, P_2 \leq P_{\max} \\ & \gamma_T \geq \Psi, \end{aligned} \quad (85)$$

where $P_{\max}$ represents the maximum power budget of the UL CUs, Ψ is the sensing target SINR threshold, and the sensing target SINR, γ_T, at the BS is given by

$$\gamma_T = \frac{\eta^2|h|^2P}{(|g_1|^2+\zeta_{U_1}^2)P_1+(|g_2|^2+\zeta_{U_2}^2)P_2+\sigma^2}. \quad (86)$$

We notice that the objective function subject to the constraints in (85) is linear, and thus, it can be numerically solved by using CVX [36], [37].

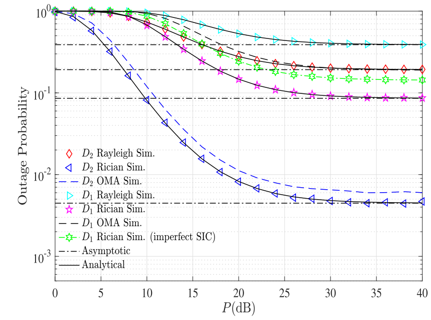

Fig. 2. OP of DL CUs D_1 and D_2 versus P.

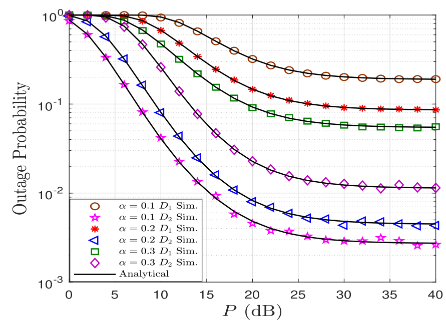

Fig. 3. OP of DL CUs vs. P for varying α.

B. Jain's Fairness Index

The Jain's fairness index measures the equality of user power allocation, and for a two-user case, it is given by

$$J = \frac{(\mathrm{R}_1+\mathrm{R}_2)^2}{2(\mathrm{R}_1^2+\mathrm{R}_2^2)}. \quad (87)$$

If $\mathrm{R}_1 = \mathrm{R}_2$, it means that both the users achieve the same rate and thus, for the max-min power allocation scheme, $J = 1$. When the users transmit with their maximum available power, the disparity between them increases, eventually decreasing the fairness, which indicates that the power allocation scheme is not optimal and, thus, $J < 1$.

VI. Results and Discussion

In this section, we discuss the numerical results for the derived analytical expressions of the given system. We consider the system parameters as $\eta = 0.9$, $\alpha = 0.2$, $\nu = 2$, $\sigma^2 = 1$, $\zeta_{D_i}^2 = \zeta_{U_i}^2 = 0.02$ for $i = 1, 2$, $d_{U_2} = d_{D_2} = d_{22} = 160$ m, $d_{U_1} = d_{D_1} = d_{11} = 80$ m and $d_S = d_T = d_{21} = d_{12} = 120$ m. Unless stated otherwise, the values of the system parameters remain unchanged for all the results. We have thoroughly verified all the analytical results through Monte-Carlo simulations.

A. Communication Performance Metrics

1) Outage Probabilities of D_1 and D_2: In Fig. 2, we have analyzed the performance of OP as a function of the transmit power P at the BS for the DL CUs D_1 and D_2 with UL user powers $P_1 = 10$ dB and $P_2 = 0.2P_1$. The UL CUs powers are intentionally kept low to minimize their interference with the DL CUs. We observe that for any fixed value of P, the probability that the system is experiencing an outage for a Rician channel is significantly lower than that for the

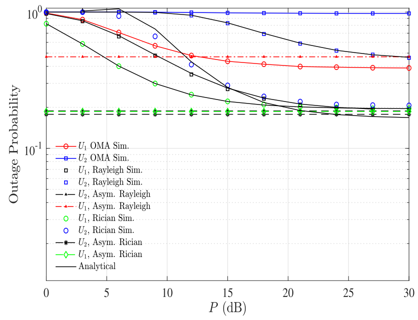

Fig. 4. OP of UL CUs versus P_1.

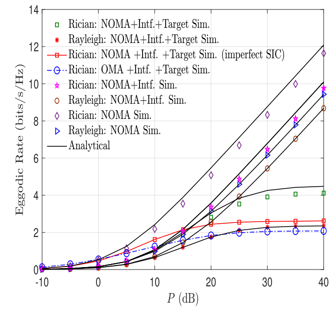

Fig. 5. DL NU $\overline{\mathrm{R}}_{D_1}$ versus P.

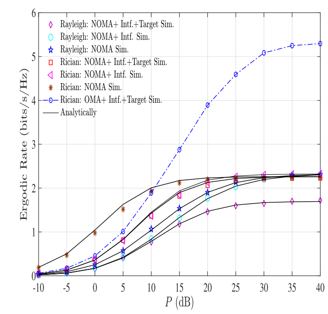

Fig. 6. DL FU $\overline{\mathrm{R}}_{D_2}$ versus P.

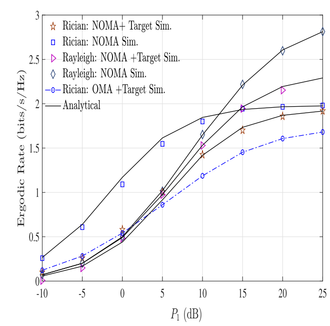

Fig. 7. UL NU $\overline{\mathrm{R}}_{U_1}$ versus P_1.

Rayleigh channel. The exact match between the analytical and simulation results determines the accuracy of our derived analytical expressions as given in (10), (17), (19) and (23). We infer that as the values of m_1 and m_2, i.e., the LoS component, increase, the outage performance improves, which is as expected. Moreover, in DL NOMA, the strong user (i.e., the near user) is affected more by the interferences, indicating poor performance as compared to the weak user (far user). We have also shown the asymptotic behaviour of the OPs for higher transmit power, $(\gamma_{i,D_i} \rightarrow \infty)$ for $i \in \{1, 2\}$, in the same figure. It can be observed from Fig. 2 that the derived analytical expressions and the asymptotic results match exactly in the high transmit power regime. Further, we have also considered a scenario where the near user is unable to perform perfect SIC, with a residual error of 0.03. In this case, the near user's performance degrades marginally compared to the perfect SIC case, while the far user's performance remains unaffected, since SIC is applied only at the near user. Moreover, we compare the proposed NOMA-aided system with its OMA-based counterpart, where it can be clearly observed that the OP for both D_1 and D_2 is significantly better with the NOMA scheme.

2) Effect of Varying Power Allocation Coefficient: In Fig. 3, we have compared the OP of DL CUs with respect to P for different values of power allocation coefficients $\alpha = 0.1$, $\alpha = 0.2$, and $\alpha = 0.3$ and for the Rician fading scenario. For fixed values of $P_1 = 10$ dB and $P_2 = 0.2P_1$, we observe that as α (near user power allocation coefficient) increases, the power allocated to the far user decreases and thus, for a particular value of SNR, the probability that user D_2 is in outage increases, whereas, it improves for D_1. The same observations can be inferred for a Rayleigh fading channel.

3) Outage Probability of U_1 and U_2: Fig. 4 shows the OP of UL CUs against the transmit power of U_1. In UL NOMA, the effect of interferences on the weak user is higher than that on the strong user. Although the BS removes the near user symbol using SIC, the far user has a lower transmit power and poor channel condition compared to the near user. Therefore, we observe that the performance of the near user U_1 is better than that of the far user U_2. This observation is in contrast to the DL scenario since the order of decoding symbols is different from that of the UL case. Using approximations in the derived analytical expressions, the numerical results of these expressions closely follow the simulation results over the Rician fading channel, whereas for the Rayleigh fading case, the analytical and simulation results exactly match. In addition, we have presented the asymptotic OP results for the high transmit power regime, $\gamma_{i,U_i} \rightarrow \infty$, for $i \in \{1, 2\}$. As shown in Fig. 4, the derived OP expressions closely match with the simulation results at lower transmit power levels and converge exactly to the asymptotic expressions as the transmit power increases. Additionally, we compare the NOMA-based system with the OMA-based system. It can be observed that the OP of U_2 is worse in the OMA-based system, whereas it is significantly better when employing the NOMA scheme. As expected, the OMA scheme performs better for the near user as compared to the far user.

4) Ergodic Rate of DL CUs: Figs. 5 and 6 depict the ergodic rate as a function of the transmit power P at the BS for DL CUs D_1 and D_2, respectively, with means $m_1 = 0.75$ and $m_2 = 1$. We assume that the UL users transmit with powers $P_1 = 0$ dB and $P_2 = 0.4\ P_1$. We observe that the ergodic rates of NOMA for a Rician channel perform better than the Rayleigh channel for all three scenarios: (i) in the presence of interferences from the UL CUs and a target, (ii) in the presence of interferences from the UL CUs only, and (iii) in the absence of a target and interferences (conventional DL NOMA transmissions without interferences). It can be inferred

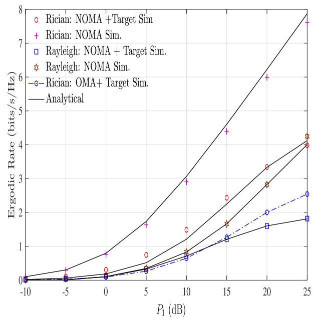

Fig. 8. UL FU $\overline{\mathrm{R}}_{U_2}$ versus P_1.

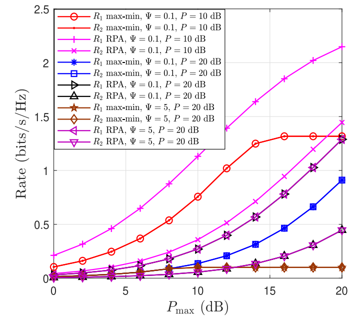

Fig. 9. UL CUs rate versus $P_{\max}$.

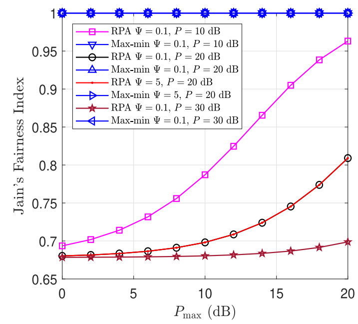

Fig. 10. Jain's fairness index versus $P_{\max}$.

that if the transmit power at the BS increases, both DL users' achievable rates will improve. Moreover, as expected, the ergodic rate of the system improves significantly for the near user D_1 in the absence of a target, and further improvement occurs when the UL CUs are not considered as interferences. Meanwhile, for the far user D_2, the effect of the interferences and target does not impact much on the rate performance in the high SNR region. Finally, the achievable rate performance of the near user D_1 is much higher than that of the far user D_2 in the DL scenario, as the SIC is applied at the near user. However, under imperfect SIC with a residual error factor of 0.03, the ergodic rate of the near user is reduced compared to the perfect SIC scenario. In addition, we compare the performance of the proposed NOMA-based system with that of an OMA-based system. It is observed that, in the DL, the near user consistently achieves better performance under NOMA compared to OMA. However, for the far user, NOMA outperforms OMA at lower transmit power levels, whereas OMA yields better performance when the transmit power is high. This occurs because, in NOMA, increasing the transmit power enhances both the desired signal and the inter-user interference. In contrast, in OMA, the use of orthogonal resource allocation ensures that only the desired signal power of the far user is enhanced.

5) Ergodic Rate of UL CUs: The ergodic rates of U_1 and U_2 as a function of CU U_1 power P_1 are shown in Figs. 7 and 8, respectively. In Fig. 7, for $P = 10$ dB, we observe that even though the achievable rate of U_1 increases in the absence of a target, the performance for a Rayleigh channel is better than the Rician channel. This is because, for the Rician faded environment, the channel conditions are better for both the users interfering with each other at the BS. Moreover, in the UL scenario, the near user is decoded against interference from the far user.

In contrast, Fig. 8 with $P = 0$ dB, the ergodic rate performance achieves a significant improvement for the Rician fading channel compared to the Rayleigh fading channel. In the presence of a target, for a given communication-to-sensing decoding order in the UL scenario of NOMA-assisted ISAC, the information of UL CUs is decoded against the sensing interference. Therefore, the communication performance degrades, and thus, the ergodic rate decreases. Furthermore, increasing the transmit power at the BS to enhance DL data rates and sensing performance leads to stronger sensing echoes. These echoes, in turn, introduce more interference at the BS, thereby reducing the achievable rates for the UL CUs. We notice that if the target is close to the BS, the interference caused by the target also increases, resulting in poor ergodic rates for UL CUs. Since SIC is applied at the BS to decode the information of the CU U_2, we observe that the ergodic rate of U_2 is better than U_1 for the UL NOMA scenario in the absence of a target. In addition, it is observed that for both UL CUs, the NOMA-based system outperforms the OMA-based system in terms of achievable rates even in the presence of target echo interference. From Figs. 7 and 8, it can be observed that due to Jensen's inequality and first-order Taylor series approximation, the approximate achievable rate causes a slight deviation in the analytical results compared to the simulation results.

6) UL Power Optimization: The instantaneous rate of the UL CUs vs $P_{\max}$ values is shown in Fig. 9. For the random power allocation (RPA), we assume $P_1 = P_{\max}$ and $P_2 = 0.4P_1$. We observe that the rate of both the UL CUs increases as the transmit power P of the BS decreases. The exact match of the rates of both the CUs for the max-min power allocation strategy proves that we have accurately solved this optimization problem using CVX. Further, increasing the SINR target threshold Ψ for the max-min power allocation significantly decreases the rate of the UL CUs. This effect, however, is not observed in the RPA case, as the rates with the RPA scheme for different values of Ψ remain the same.

7) Jain's Fairness Index: Fig. 10 shows the Jain's fairness index for different values of $P_{\max}$. For the RPA scheme, we assume $P_1 = P_{\max}$ and $P_2 = 0.4P_1$. We observe that irrespective of the target SINR threshold Ψ and transmit power P of the BS, the fairness index for the max-min power allocation is always 1, indicating the maximum fairness among the near and far CUs in the UL scenario. Also, the fairness index decreases as P increases. This is because the performance of the DL devices increases while simultaneously improving the sensing performance of the system. For example, from Fig. 10,

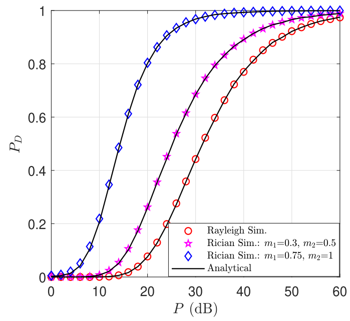

Fig. 11. Detection probability P_D versus P.

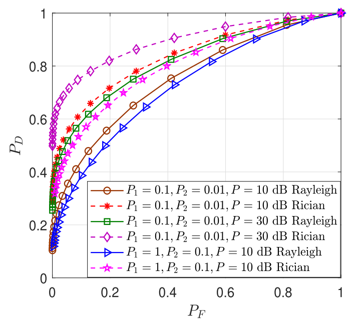

Fig. 12. ROC: P_D versus P_F.

for the RPA scheme when $P = 30$ dB, the fairness index is the least compared to the lesser transmit powers of the BS. Also, it can be observed that Ψ does not have any effect on the fairness index of the UL CUs as long as P remains the same; however, the rate decreases with increasing Ψ. These observations can be verified from Fig. 10 for $\Psi = 0.1$ and 5 with $P = 20$ dB.

B. Sensing Performance Metrics

1) Target Detection Probability: The probability of target detection against the transmit power P of the BS is illustrated in Fig. 11. Assuming $P_1 = 0$ dB and $P_2 = 0.4P_1$, the probability of detecting the target in a Rician fading scenario is shown in the figure and compared with that of the Rayleigh fading environment. Due to the presence of the LoS component in the Rician channel, we observe higher detection probability can be achieved at lower values of P. At $P =$ 20 dB, P_D for a Rician fading channel with $m_1 = 0.3$ and $m_2 = 0.5$ is more than three times that of a Rayleigh channel. The exact match between analysis and simulation verifies our theoretical derivation of P_F and P_D as shown in (81) and (82), respectively. Also, an increase in the value of m_1 and m_2 will lead to a higher detection probability, indicating a better and improved sensing performance of the system.

2) Receiver Operating Characteristics: In Fig. 12, we have shown the probability of detection P_D versus the false alarm probability P_F for different values of P_1, P_2, and P. It is also referred to as the receiver operating characteristic (ROC), which analyzes the sensing performance of the system. For threshold $\varrho = 0$, the NP detector always determines $\mathcal{H}_1$ and thus, $P_D = P_F = 1$. As the value of ϱ increases, both P_D and P_F decrease. These observations have been shown for both Rician and Rayleigh fading channels. It can be inferred that if the power at the BS increases from $P = 10$ dB to $P = 30$ dB, then for a fixed value of $P_F = 0.2$ and Rayleigh fading scenario, the detection probability increases from 0.56 to 0.72. This indicates that the sensing performance of the system increases as the transmit power of the BS increases. We also observe that for a fixed $P = 10$ dB and $P_F = 0.2$, the detection probability decreases when the transmit power of the UL CUs increases. We observe that as the transmit power of the BS increases, a higher AUC is achieved, and simultaneously, the communication performance of the system for the DL CUs improves. When the UL CUs transmit with a higher power, the sensing performance degrades as a lower AUC is obtained. Also, the interference caused by these UL devices on the DL users will degrade the communication performance of the DL CUs.

VII. Conclusion

This paper derived the analytical framework considering DL and UL communication users together in the presence of a radar target and interferences for a realistic and practical Rician fading channel. Specifically, we derived the closed-form expressions of the outage probabilities for both the near and far users in the DL and UL scenarios. Also, the asymptotic expressions have been derived and provide insights into the OPs' saturation levels. We observed that obtaining the closed-form expressions of the ergodic rates through the derived CDF expressions is mathematically intractable. Therefore, the approximate expressions of the achievable rates have been obtained, and we observed that these analytical expressions closely follow the Monte-Carlo simulations. The detection and false-alarm probabilities have been derived for our system, and the ROC were employed to illustrate the performance of the target detector. Furthermore, to achieve user fairness, the max-min power allocation optimization problem has been utilized for the UL scenario under a service constraint for the radar. We investigated the performance tradeoff between communication and sensing functionalities through the derived analytical and numerical results while simultaneously demonstrating NOMA as a potential candidate for an ISAC system as compared to the OMA scheme. A thorough performance analysis comparison has been presented between the Rician and Rayleigh fading environments. In general, deriving closed-form expressions for the performance metrics to gain insights into the proposed wireless system is more challenging for the uplink communication users than for the downlink case, mainly due to the involvement of the target echo received at the base station.

References

[1] H. Griffiths, S. Blunt, L. Cohen, and L. Savy, "Challenge problems in spectrum engineering and waveform diversity," in *Proc. IEEE Radar Conf. (RadarCon)*, Ottawa, ON, Canada, Apr. 2013, pp. 1–5.

[2] F. Liu, C. Masouros, A. P. Petropulu, H. Griffiths, and L. Hanzo, "Joint radar and communication design: Applications, state-of-the-art, and the road ahead," *IEEE Trans. Commun.*, vol. 68, no. 6, pp. 3834–3862, Jun. 2020.

[3] D. K. Pin Tan et al., "Integrated sensing and communication in 6G: Motivations, use cases, requirements, challenges and future directions," in *Proc. 1st IEEE Int. Online Symp. Joint Commun. Sens.*, Dresden, Germany, Feb. 2021, pp. 1–6.

[4] F. Wang and H. Li, "Joint power allocation for radar and communication co-existence," *IEEE Signal Process. Lett.*, vol. 26, no. 11, pp. 1608–1612, Nov. 2019.

[5] F. Liu et al., "Integrated sensing and communications: Toward dual-functional wireless networks for 6G and beyond," *IEEE J. Sel. Areas Commun.*, vol. 40, no. 6, pp. 1728–1767, Jun. 2022.

[6] J. A. Zhang et al., "Enabling joint communication and radar sensing in mobile networks—A survey," *IEEE Commun. Surveys Tuts.*, vol. 24, no. 1, pp. 306–345, 1st Quart., 2022.

[7] Q. Zhang, H. Sun, X. Gao, X. Wang, and Z. Feng, "Time-division ISAC enabled connected automated vehicles cooperation algorithm design and performance evaluation," *IEEE J. Sel. Areas Commun.*, vol. 40, no. 7, pp. 2206–2218, Jul. 2022.

[8] Z. He, W. Xu, H. Shen, D. W. K. Ng, Y. C. Eldar, and X. You, "Full-duplex communication for ISAC: Joint beamforming and power optimization," *IEEE J. Sel. Areas Commun.*, vol. 41, no. 9, pp. 2920–2936, Sep. 2023.

[9] C. Ouyang, Y. Liu, and H. Yang, "Performance of downlink and uplink integrated sensing and communications (ISAC) systems," *IEEE Wireless Commun. Lett.*, vol. 11, no. 9, pp. 1850–1854, Sep. 2022.

[10] X. Mu, Z. Wang, and Y. Liu, "NOMA for integrating sensing and communications towards 6G: A multiple access perspective," *IEEE Wireless Commun.*, vol. 31, no. 3, pp. 316–323, Jun. 2024.

[11] Y. Saito, Y. Kishiyama, A. Benjebbour, T. Nakamura, A. Li, and K. Higuchi, "Non-orthogonal multiple access (NOMA) for cellular future radio access," in *Proc. IEEE 77th Veh. Technol. Conf. (VTC Spring)*, Dresden, Germany, Jun. 2013, pp. 1–5.

[12] X. Liu, H. Liu, K. Zheng, J. Liu, T. Taleb, and N. Shiratori, "AoI-minimal clustering, transmission and trajectory co-design for UAV-assisted WPCNs," *IEEE Trans. Veh. Technol.*, vol. 74, no. 1, pp. 1035–1051, Jan. 2025.

[13] X. Mu, Z. Wang, and Y. Liu, "NOMA for integrating sensing and communications toward 6G: A multiple access perspective," *IEEE Wireless Commun.*, vol. 31, no. 3, pp. 316–323, Jun. 2024.

[14] Z. Wang, Y. Liu, X. Mu, Z. Ding, and O. A. Dobre, "NOMA empowered integrated sensing and communication," *IEEE Commun. Lett.*, vol. 26, no. 3, pp. 677–681, Mar. 2022.

[15] C. Ouyang, Y. Liu, and H. Yang, "On the performance of uplink ISAC systems," *IEEE Commun. Lett.*, vol. 26, no. 8, pp. 1769–1773, Aug. 2022.

[16] C. Zhang, W. Yi, and Y. Liu, "Semi-integrated-sensing-and-communication (Semi-ISaC) networks assisted by NOMA," in *Proc. IEEE Int. Conf. Commun.*, Seoul, South Korea, May 2022, pp. 3790–3795.

[17] C. Ouyang, Y. Liu, and H. Yang, "Revealing the impact of SIC in NOMA-ISAC," *IEEE Wireless Commun. Lett.*, vol. 12, no. 10, pp. 1707–1711, Oct. 2023.

[18] C. Ouyang, X. Zhang, and Y. Liu, "Performance analysis of downlink NOMA-ISAC," in *Proc. IEEE Global Commun. Conf.*, Kuala Lampur, Malaysia, Dec. 2023, pp. 7393–7398.

[19] Z. Wang, Y. Liu, X. Mu, and Z. Ding, "NOMA inspired interference cancellation for integrated sensing and communication," in *Proc. IEEE Int. Conf. Commun.*, Seoul, South Korea, May 2022, pp. 3154–3159.

[20] M. Liu, M. Yang, and A. Nallanathan, "On the performance of uplink and downlink integrated sensing and communication systems," in *Proc. IEEE Globecom Workshops (GC Wkshps)*, Rio de Janeiro, Brazil, Dec. 2022, pp. 1236–1241.

[21] M. Liu et al., "A nonorthogonal uplink/downlink IoT solution for next-generation ISAC systems," *IEEE Internet Things J.*, vol. 11, no. 5, pp. 8224–8239, Mar. 2024.

[22] I. Agrawal and B. R. Manoj, "Ergodic rate for downlink and uplink NOMA aided integrated sensing and communication," *IEEE Commun. Lett.*, vol. 28, no. 12, pp. 2774–2778, Dec. 2024.

[23] R. Jiao, L. Dai, J. Zhang, R. MacKenzie, and M. Hao, "On the performance of NOMA-based cooperative relaying systems over Rician fading channels," *IEEE Trans. Veh. Technol.*, vol. 66, no. 12, pp. 11409–11413, Dec. 2017.

[24] F. B. Hildebrand, *Introduction to Numerical Analysis*. New York, NY, USA: Dover, 1987.

[25] J. G. Proakis, *Digital Communications*, 5th ed., New York, NY, USA: McGraw-Hill, 2007.

[26] S. Choudhury and J. D. Gibson, "Information transmission over fading channels," in *Proc. IEEE Global Telecommun. Conf. (GLOBECOM)*, Washington, DC, USA, Nov. 2007, pp. 3316–3321.

[27] S. András, Á. Baricz, and Y. Sun, "The generalized Marcum Q-function: An orthogonal polynomial approach," 2010, *arXiv:1010.3348*.

[28] A. Nuttall, "Some integrals involving the Q_M function (corresp.)," *IEEE Trans. Inf. Theory*, vol. 21, no. 1, pp. 95–96, Jan. 1975.

[29] I. S. Gradshteyn and I. M. Ryzhi, *Table of Integrals, Series, and Products*, 7th ed., San Diego, CA, USA: Academic, 2007.

[30] M. K. Simon, *Probability Distributions Involving Gaussian Random Variables: A Handbook for Engineers and Scientists*. Cham, Switzerland: Springer, 2002.

[31] P. K. Hota, S. Thapar, D. Mishra, R. Saini, and A. Dubey, "Ergodic performance of downlink untrusted NOMA system with imperfect SIC," *IEEE Commun. Lett.*, vol. 26, no. 1, pp. 23–26, Jan. 2022.

[32] M. Liu et al., "Performance analysis and power allocation for cooperative ISAC networks," *IEEE Internet Things J.*, vol. 10, no. 7, pp. 6336–6351, Apr. 2023.

[33] L. Zhang, J. Liu, M. Xiao, G. Wu, Y.-C. Liang, and S. Li, "Performance analysis and optimization in downlink NOMA systems with cooperative full-duplex relaying," *IEEE J. Sel. Areas Commun.*, vol. 35, no. 10, pp. 2398–2412, Oct. 2017.

[34] H. L. Van Trees, *Detection, Estimation, and Modulation Theory, Part I: Detection, Estimation, and Linear Modulation Theory*. Hoboken, NJ, USA: Wiley, 2004.

[35] D. W. Bliss and S. Govindasamy, *Adaptive Wireless Communications*. Cambridge, MA, USA: Wellesley-Cambridge, 2013.

[36] M. Grant and S. Boyd. (Mar. 2014). *CVX: MATLAB Software for Disciplined Convex Programming, Version 2.1*. [Online]. Available: https://cvxr.com/cvx

[37] M. Grant and S. Boyd, "Graph implementations for nonsmooth convex programs," in *Recent Advances in Learning and Control* (Lecture Notes in Control and Information Sciences). Cham, Switzerland: Springer, 2008, pp. 95–110. [Online]. Available: http://stanford.edu/~boyd/graph_dcp.html

Ishaan Agrawal received the B.Tech. degree in electronics and communication engineering from the Vellore Institute of Technology, Vellore, India, in 2022, and the M.Tech. degree in communication engineering from the Indian Institute of Technology Guwahati, Guwahati, India, in 2024. He is currently an Embedded Software Engineer with Analog Devices India Pvt., Ltd., Bengaluru, India, since July 2024. His research interests include multiple-access techniques, next-generation wireless communications, and integrated sensing and communication.

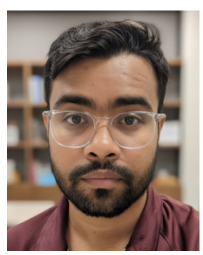

Harsh Raj (Student Member, IEEE) received the B.E. degree in electronics and communication engineering from the University Institute of Technology, Burdwan, India, in 2019, and the M.Tech. degree in communication and signal processing from the Indian Institute of Technology Ropar, India, in 2022. He is currently pursuing the Ph.D. degree with the Department of Electronics and Electrical Engineering, Indian Institute of Technology Guwahati, India. His research interests include next-generation wireless communications, multiple-access techniques, joint sensing and communication, intelligent reflecting surfaces, and the application of deep learning and machine learning in wireless systems.

B. R. Manoj (Senior Member, IEEE) received the B.E. degree in electronics and communication engineering from the Visvesvaraya Technological University, India, in 2007, the M.Tech. degree in signal processing from the Indian Institute of Technology Guwahati, Guwahati, in 2011, and the Ph.D. degree from the Indian Institute of Technology Delhi, New Delhi, in 2019. He was a Member Technical Staff with the Saankhya Labs Pvt., Ltd., Bengaluru, India; a Marie-Curie Early Stage Researcher with the Athens Information Technology, Athens, Greece; an Early Doctoral Research Fellow with the Indian Institute of Technology Delhi; a Post-Doctoral Researcher with the Division of Communication Systems, Department of Electrical Engineering, Linköping University, Sweden; and a Senior Researcher with the Radio Transmission Technology Lab, Huawei Technologies, Stockholm, Sweden. Since December 2021, he has been with the Department of Electronics and Electrical Engineering, Indian Institute of Technology Guwahati, where he is currently an Assistant Professor. His research interests include wireless communication and networks, signal processing and machine learning for communications, adversarial machine learning, and Markov chains and their applications.